Remote Sensing of Environment 248 (2020) 112003

Contents lists available at ScienceDirect

Remote Sensing of Environment

journal homepage: www.elsevier.com/locate/rse

Monitoring biochemical limitations to photosynthesis in N and P-limited radiata pine using plant functional traits quantified from hyperspectral imagery

Michael S. Watt[a,*], Henning Buddenbaum[b], Ellen Mae C. Leonardo[c], Honey Jane Estarija[c], Horacio E. Bown[d], Mireia Gomez-Gallego[e], Robin J.L. Hartley[c], Grant D. Pearse[c], Peter Massam[c], Liam Wright[c], Pablo J. Zarco-Tejada[f,g]

[a] Scion, 10 Kyle St, Christchurch 8011, New Zealand
[b] Environmental Remote Sensing and Geoinformatics, Trier University, 54286 Trier, Germany
[c] Scion, PO Box 3020, Rotorua, New Zealand
[d] Faculty of Forestry, Universidad de Chile, Casilla 9206, Santiago, Chile
[e] Department of Forest Mycology and Plant Pathology, Swedish University of Agricultural Sciences, Box 7026, 750 07 Uppsala, Sweden
[f] The University of Melbourne, Melbourne, Victoria 3010, Australia
[g] Instituto de Agricultura Sostenible (IAS), Consejo Superior de Investigaciones Científicas (CSIC), Alameda del Obispo s/n, 14004 Cordoba, Spain.

ARTICLE INFO

Keywords:
High resolution hyperspectral
J_{max}
N:P ratio
Nutrient limitation
Physically based models
Radiative transfer
Reflectance
V_{cmax}

ABSTRACT

The prediction of carbon uptake by forests across fertility gradients requires accurate characterisation of how biochemical limitations to photosynthesis respond to variation in key elements such as nitrogen (N) and phosphorus (P). Over the last decade, proxies for chlorophyll and photosynthetic activity have been extracted from hyperspectral imagery and used to predict important photosynthetic variables such as the maximal rate of carboxylation (V_{cmax}) and electron transport (J_{max}). However, little research has investigated the generality of these relationships within the nitrogen (N) and phosphorus (P) limiting phases, which are characterised by mass based foliage ratios of N:P $\leq$ 10 for N limitations and N:P $>$ 10 for P limitations.

Using measurements obtained from one year old *Pinus radiata* D. Don grown under a factorial range of N and P treatments this research examined relationships between photosynthetic capacity (V_{cmax}, J_{max}) and measured N, P and chlorophyll (Chl_{a+b}). Using functional traits quantified from hyperspectral imagery we then examined the strength and generality of relationships between photosynthetic variables and Photochemical Reflectance Index (PRI), Sun-Induced Chlorophyll Fluorescence (SIF) and chlorophyll $a + b$ derived by radiative transfer model inversion.

There were significant ($P < .001$) and strong relationships between photosynthetic variables and both N ($R^2 = 0.82$ for V_{cmax}; $R^2 = 0.87$ for J_{max}) and Chl_{a+b} ($R^2 = 0.85$ for V_{cmax}; $R^2 = 0.86$ for J_{max}) within the N limiting phase that were weak ($R^2 < 0.02$) and insignificant within the P limiting phase. Similarly, there were significant ($P < .05$) positive relationships between P and photosynthetic variables ($R^2 = 0.50$ for V_{cmax}; $R^2 = 0.58$ for J_{max}) within the P limiting phase that were insignificant and weak ($R^2 < 0.33$) within the N limiting phase.

Predictions of photosynthetic variables using Chl_{a+b} estimated by model inversion were significant ($P < .001$), positive and strong ($R^2 = 0.64$ for V_{cmax}; $R^2 = 0.63$ for J_{max}) within the N limiting phase but insignificant and weak ($R^2 < 0.05$) within the P limiting phase. In contrast, both SIF and PRI exhibited moderate to strong positive correlations with photosynthetic variables within both the N and P limiting phases. These results suggest that quantified SIF and PRI from hyperspectral images may have greater generality in predicting biochemical limitations to photosynthesis than proxies for N and chlorophyll $a + b$, particularly under high foliage N content, when P is limiting.

* Corresponding author.
E-mail address: michael.watt@scionresearch.com (M.S. Watt).

https://doi.org/10.1016/j.rse.2020.112003
Received 17 April 2020; Received in revised form 10 July 2020; Accepted 13 July 2020

1. Introduction

The use of optical data to predict biochemical, structural and physiological traits from leaves and plant canopies has increased rapidly over the last two decades (for reviews see Hill et al., 2019; Watt et al., 2019). Key attributes of interest that have been successfully estimated include water content (Buddenbaum et al., 2011; Buddenbaum et al., 2015; Colombo et al., 2008; Fang et al., 2017; Malenovský et al., 2006; Riaño et al., 2005), leaf morphological traits such as specific leaf area (Asner and Martin, 2008) and leaf mass per area (Asner et al., 2011b; Doughty et al., 2011), pigments such as chlorophyll (Croft et al., 2014; Curran et al., 2001; Gitelson et al., 1996; Tsay et al., 1982; Yoder and Pettigrew-Crosby, 1995; Zarco-Tejada et al., 2019), carotenoids (Hernández-Clemente et al., 2012; Hernández-Clemente et al., 2014) and foliar concentrations of most key nutrients, particularly nitrogen (N) and phosphorus (P) (Asner and Martin, 2008; Asner et al., 2011a; Curran et al., 2001; Dechant et al., 2017; Gillon et al., 1999; Luther and Carroll, 1999; Masaitis et al., 2014; Petisco et al., 2005; Schlerf et al., 2010; Serbin et al., 2014; Stein et al., 2014; Tsay et al., 1982; Wang et al., 2018; Wang et al., 2015; Yoder and Pettigrew-Crosby, 1995). However, the remote sensing of attributes associated with photosynthesis has progressed at a far slower rate.

The rate of carbon assimilation under ambient conditions (A) is strongly influenced by light intensity, air temperature, water availability and leaf biochemistry (Farquhar et al., 1980; Leuning, 1995). These factors have been combined into a C_3 photosynthesis model that shows the rate of carbon assimilation to be limited under ambient conditions by the maximal rate of ribulose-1,5-bisphosphate (RuBP) carboxylase-oxygenase (Rubisco) carboxylation (V_{cmax}) and the maximal electron transport rate driving regeneration of RuBP (J_{max}). In combination V_{cmax} and J_{max} define the plants biochemical limitations to photosynthesis and these two variables will be, hereafter, collectively termed photosynthetic capacity.

Previous research shows that photosynthetic capacity ranges widely both within and among species, and is sensitive to variation in environmental conditions (Groenendijk et al., 2011; Xu and Baldocchi, 2003). Despite this variation, a fixed value for V_{cmax} is often assumed in Terrestrial Biosphere Models which provide the main means of predicting regional and global estimates of terrestrial carbon (Beer et al., 2010). Many studies have investigated the use of plant functional traits such as leaf phosphorus (P), specific leaf area (SLA) and leaf nitrogen (N) to account for variation in photosynthetic capacity (Walker et al., 2014). As N is a primary component of Rubisco and the light-harvesting complexes that regulate photosynthesis (Niinemets and Tenhunen, 1997), studies have often successfully used N to predict photosynthetic capacity (Dechant et al., 2017), although seasonal variation in partitioning of N to photosynthetic fractions can complicate predictions (Croft et al., 2017). Chlorophyll content has also been found to be a useful predictor of photosynthetic capacity (Croft et al., 2017) as this pigment is involved in light harvesting and there is a direct relationship between this pigment and J_{max} (Collatz et al., 1991; Sellers et al., 1992), which in turn is usually strongly and linearly related to V_{cmax}, across a large range of species (Medlyn et al., 2002).

Chlorophyll fluorescence has been widely shown to serve as a proxy for electron transport rate and photosynthetic activity (Genty et al., 1989; Weis and Berry, 1987). As chlorophyll fluorescence is dependent on chlorophyll concentration, which has been found to be closely aligned to photosynthetic capacity (Croft et al., 2017; Houborg et al., 2013), a strong link has also been shown between Sun Induced Chlorophyll Fluorescence (SIF) and V_{cmax} (Rascher et al., 2015). A recent review has outlined the progress in SIF retrievals over the last 50 years (Mohammed et al., 2019) and research has demonstrated the utility of SIF in predicting photosynthetic activity at both the leaf and the canopy scales from a range of remote sensing platforms (Cendrero-Mateo et al., 2015; Zarco-Tejada et al., 2013a; Zarco-Tejada et al., 2016).

A parallel line of investigation over the last two decades has focussed on the use of Photochemical Reflectance Index (PRI) to predict photosynthetic activity of vegetation. This index, which is determined from narrow band reflectance at 531 and 570 nm (Gamon et al., 1992; Gamon et al., 1997) and in closely related bands in derivative versions (Gamon et al., 1993), has been widely used to predict photosynthetic status across a range of vegetation types. PRI provides a linkage with the efficiency of photosystem II through characterising variation in xanthophyll pigments and as such quantifies changes in non-photochemical quenching and light use efficiency (Gamon et al., 1997). This index has been successfully used to predict photosynthetic rate (Drolet et al., 2008; Fuentes et al., 2006; Gamon et al., 1997; Guo and Trotter, 2004; Hilker et al., 2008; Middleton et al., 2009; Nichol et al., 2000; Penuelas et al., 1995; Stylinski et al., 2000) and the photosynthetic response of plants subject to a range of stresses (Dobrowski et al., 2005; Hernández-Clemente et al., 2011; Scholten et al., 2019; Suárez et al., 2008) and is responsive to seasonal changes in pigments (Gitelson et al., 2017). PRI can be readily used to scale photosynthesis to the canopy level as recently launched satellite based hyperspectral imagers (e.g. PRISMA, DESIS) and planned missions (e.g. EnMAP) are capable of measuring this variable. In addition, Sentinel-2 and in particular the Sentinel-3 satellite OLCI and SLSTR sensors enable the estimation of vegetation pigments using the red edge spectral region and spectral bands centered at the green region for the assessment of the xanthophyll pigment dynamics and V_{cmax} at global scales using the SCOPE model (Prikaziuk and van der Tol, 2019). Although many studies show that PRI is an effective proxy for photosynthesis (Hernández-Clemente et al. 2019) the index has been shown to be affected by canopy structure, leaf pigments and background (Suárez et al., 2009; Suárez et al., 2008), which can negatively impact predictions of photosynthesis (Rascher and Pieruschka, 2008).

In this context, physically based modelling has been widely used as a method for generalising the spatial prediction of important vegetation traits. As these models are able to account for the influence of variations in background, canopy architecture and conditions during the image acquisition on reflectance they can be more generally applied than other approaches (Hill et al., 2019; Watt et al., 2019). One of the most widely used models is PROSAIL which uses PROSPECT (Jacquemoud and Baret, 1990) to simulate leaf reflectance and transmittance which are then fed into SAIL (Verhoef, 1984), which predicts canopy reflectance from this input and soil optical properties and illumination geometry (Berger et al., 2018). When PROSAIL is run in inverse mode this model can be used to predict chlorophyll content and other biochemical constituents of foliage from canopy reflectance (Le Maire et al., 2008; Zarco-Tejada et al., 2004b; Zhang et al., 2005). Given the importance of chlorophyll in the photosynthetic process, predictions of this pigment from PROSAIL have considerable potential for spatially describing variation in key photosynthetic variables. As described in the review by Jacquemoud et al. (2009) PROSAIL has been developed for homogeneous and uniform canopies, and requires more complex approximations to account for forest architecture. For this purpose, radiative transfer approaches such as DART (Gastellu-Etchegorry et al., 1996), 4-Scale (Chen et al., 1997) and FLIGHT (North, 1996) have been used with success but these require a large number of inputs.

Considerable research has demonstrated that N and P independently limit both plant growth and photosynthetic capacity and that the N:P ratio can be used to partition ranges that are either limited by N or P (Bown et al., 2007; Domingues et al., 2010; Ingestad, 1971, 1979; Ingestad and Lund, 1986). The underlying premise of this approach is that a N:P ratio of 10 (Knecht and Göransonn, 2004) marks a threshold and deviations from this lead to nitrogen (N:P $\leq$ 10) or phosphorus (N:P $>$ 10) deficiencies (Aerts and Chapin, 2000; Marschner, 1995; Reich and Schoettle, 1988). This assumption of independent limitations clearly influences how models linking photosynthetic capacity to predictors derived from hyperspectral data are interpreted. These hyperspectral predictors may have a stronger association with photosynthetic capacity within either the N or P limiting range or alternatively could

be applied using a single equation across both ranges. Despite this, we are unaware of any research that has examined how generalisable relationships between key hyperspectral variables and photosynthetic capacity are within N and P limiting ranges.

Within the southern hemisphere *Pinus radiata* D. Don (radiata pine) is the most widely planted plantation species and is particularly abundant within New Zealand where it constitutes 90% of the 1.7 M ha plantation area (NZFOA, 2018). A key limitation of photosynthesis and growth in *P. radiata* plantations is nutrient supply (Raison and Myers, 1992; Sheriff et al., 1986; Watt et al., 2005) and previous research has established relationships between V_{cmax}, J_{max} and foliar concentration of N and P in this species (Bown et al., 2007; Walcroft et al., 1997). However, we are unaware of any research that has investigated the utility of hyperspectral imagery for predicting photosynthetic capacity in *P. radiata*.

In this study, measurements of hyperspectral imagery, foliage nutrition and photosynthesis were taken from an experiment that included a factorial combination of N and P treatments applied to *P. radiata*. Using this data, the overall goal of this research was to better understand the key determinants of photosynthetic capacity and how hyperspectral imagery can best be used to predict photosynthetic capacity. Specifically, we examined relationships between photosynthetic capacity and measured chlorophyll (Chl_{a+b}), N and P within both the N and P limiting ranges. Using plant functional traits derived from hyperspectral data we then explored the strength and generality of relationships between photosynthetic capacity and PRI, SIF and chlorophyll $a + b$ derived by radiative transfer model inversion.

2. Methods

2.1. Experimental set up

The experiment was undertaken within the Scion nursery, located in Rotorua, New Zealand. A total of 120 *P. radiata* seedlings were transplanted into pots with a 15 l volume during October 2018. The medium into which the plants were transplanted consisted of a mixture of perlite and vermiculite which are silica-based products without any nutritional content. Plants were grown in a thermostatically controlled greenhouse where temperature in spring fluctuated between 10 and 24 °C during the day and between 10 and 16 °C during the night. These plants were watered weekly over the duration of the trial so that root-zone water content did not limit growth. This study reports on detailed measurements taken from a subsample of 30 trees, within this trial, that included six trees from each of the five treatments.

The five fertiliser treatments consisted of a factorial combination of N and P that were applied as 500 ml of nutrient solution per plant every fortnight starting on the 20th February 2019. These five treatments included application of water only (Control), low N–low P (N0P0), low N–high P (N0P1), high N–low P (N1P0) and high N–high P (N1P1). Nutrient solutions consisted of two levels of nitrogen (N0 = 1.43 and N1 = 7.14 mol m^{-3}) and phosphorus (P0 = 0.084 and P1 = 0.420 mol m^{-3}). Following Ingestad (1979) N was provided at concentrations of 100 ppm (7.14 mM) and P at 13 ppm (0.420 mM) as the high-N and high-P supply regimes. The low-N (1.43 mM) and low-P (0.084 mM) supply regimes were chosen as one-fifth of the high-N and high-P concentrations, respectively. Nitrogen was supplied as NH_4NO_3 and phosphorus as KH_2PO_4 and nutrients other than N and P were provided in optimum proportions in relation to N, as defined by Ingestad (Ingestad, 1971, 1979).

2.2. Hyperspectral data capture

2.2.1. Data capture

A hyperspectral camera (FX10, Specim, Spectral Imaging Ltd., Oulu, Finland) was used to acquire hyperspectral imagery outside of the greenhouse, under clear sky conditions, from 10:30 am to 1:30 pm on the 4th October 2019. This push-broom camera captures 448 bands with wavelengths ranging from 400 to 1000 nm with a spectral full width at half maximum (FWHM) of 5.5 nm. The camera is designed for industrial applications and as such has a high maximum frame rate of 9900 frames per second with one band, and 330 frames per second using the full range of bands, as well as a high Signal-to-Noise Ratio (SNR) of 600:1. Within the field of view of 38° the spatial sampling comprises 1024 pixels. We used the Lumo Recorder software interface to manage the image acquisition.

The camera was mounted 2 m above ground on a cross beam that was supported by two posts, and a conveyor belt was used to move the plants through the field of view. The speed of the conveyor belt was adapted to fit the frame rate of the camera, which in turn was dependent on the exposure time, which had to be adjusted to the current illumination conditions. During the measurements, the conveyor belt speed and frame rate were kept constant and the exposure time was adjusted to avoid over or undersaturation. A diffuse white reference standard (Spectralon, North Hutton, NH, USA) was placed so that it was visible in every frame allowing calibration of the imagery as a function of the changing illumination conditions.

2.2.2. Pre-processing of hyperspectral data

All pre-processing of the hyperspectral data was carried out using Matlab (The MathWorks, Inc., Natick, Massachusetts, United States) following the methods described in Buddenbaum et al. (2019). Pixels with NDVI ≥0.5 and reflectance at 780 nm ≥ 0.2 were selected as

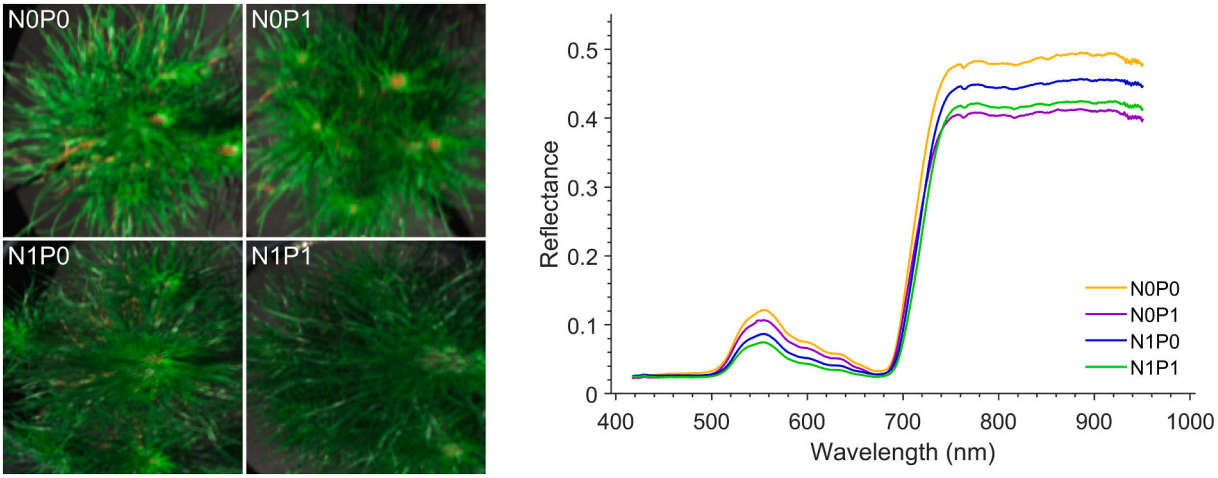

Fig. 1. Images of individual trees selected from the treatments (left) and their corresponding canopy reflectance (right).

vegetation pixels. Pixels with absolute first difference values ≥0.1 were masked out. Sample reflectance spectra for trees that are representative of the treatments are shown in Fig. 1. Following these steps the number of pixels selected ranged from 16,000–112,000 pixels/tree, with an average of 52,267 pixels/tree. The mean of all pixels for each tree was calculated to represent the whole plant.

Following these steps, the tree level spectra were smoothed using the Savitzky-Golay filter (Mouazen et al., 2010) as this filter has consistently been found to be one of the best available pre-processing transformations (Vasques et al., 2008). This smoothing used a third order polynomial which was applied across a moving window of 27 spectral bands. Reflectance and the 1st derivative of reflectance were extracted from these smoothed spectra. As there was considerable noise at either end of the smoothed spectral data, the 52 bands that occurred both below 415 nm and above 951 nm, were excluded from further analyses. Following these exclusions, 396 bands (415–951 nm) describing reflectance and 395 bands (416–951 nm) describing the 1st derivative of reflectance were available for analyses.

2.2.3. Radiative transfer model inversion

Pure vegetation reflectance spectra extracted from the hyperspectral data acquired from the seedlings was used to invert PROSAIL to estimate chlorophyll $a + b$ content ($Chl_{a+b\ PROSAIL}$). Although SAIL is designed for homogeneous canopies and this condition was not met by our experimental set-up, an inversion of PROSAIL was undertaken (Jacquemoud et al., 2009) using the spectra extracted from pure vegetation pixels (as in Zarco-Tejada et al., 2018). The PROSPECT model has been demonstrated to be valid for simulating needle reflectance in Jack Pine (*Pinus banksiana* Lamb.) stands for chlorophyll $a + b$ content estimation (Zarco-Tejada et al., 2004a). The proposed PROSPECT and SAIL models used here were successful for chlorophyll content estimation when targeting pure vegetation pixels in forest areas (Zarco-Tejada et al., 2001). Thus, we used a combination of PROSPECT-D (Féret et al., 2017) and 4SAIL (Verhoef et al., 2007) model versions, and inverted the spectra using the function lsqcurvefit in Matlab, following an approach by Jay et al. (2016). Parameters with low sensitivity were fixed so that only a limited number of parameters needed to be optimized. The leaf inclination distribution type was set to 2 so that only the average leaf inclination angle (ALA) was included in the model. The soil spectrum was also fixed. The model code includes spectra for a dark wet and a bright dry soil. We used a linear combination of 10% dark soil and 90% bright soil. Further model parameters are listed in Table 1.

Table 1
Model parameters used within PROSAIL.

Variable parameters				
Parameter	Symbol	Unit	Min	Max
Mesophyll structure parameter	N		1.4	1.6
Chlorophyll a + b	Chl_{a+b}	μg cm^{-2}	25	60
Carotenoids	C_{cx}	μg cm^{-2}	1	15
Anthocyanins	C_{anth}	μg cm^{-2}	0	5
Water content	C_w	g cm^{-2}	0.0002	0.06
Dry matter content	C_m	g cm^{-2}	0.0001	0.03
Average leaf inclination angle	ALA (LIDFa)	°	0	90
Leaf area index	LAI		0.5	5

Fixed parameters			
Parameter	Symbol	Unit	Value
Brown pigments	C_{bp}		0
Hot spot parameter	*Hot*		0.1
Observation zenith angle	θ_o	°	0
Illumination zenith angle	θ_s	°	45
Relative azimuth angle	ψ	°	0

2.2.4. Calculation of PRI and sun induced chlorophyll fluorescence

The reflectance spectra were interpolated to a 1 nm resolution within Matlab. Using the interpolated spectra, calculations of PRI ($PRI_{531,570}$) were made using the following (Gamon et al., 1992),

$$PRI = (R_{531} - R_{570})/(R_{531} + R_{570}) \quad (1)$$

We also trialled an alternative formulation of PRI ($PRI_{528,567}$) that utilised 528 nm and 567 nm (Gamon et al., 1993) and this variation was used in analyses as it was more precisely correlated to photosynthetic capacity than $PRI_{531,570}$. Although PRI was developed to track changes in xanthophyll pigments, it has been reported that such spectral bands in the 530–570 nm region are also influenced by confounding effects related to the absorption of other photosynthetic pigments, structure of the canopy, and the soil and background (Suárez et al., 2009; Suárez et al., 2008; Zarco-Tejada et al., 2013b). Thus, changes observed in PRI are potentially due to the combined changes of chlorophyll and xanthophylls, and structural effects over the course of the experiment.

Sun-Induced Chlorophyll Fluorescence (SIF) was quantified using the 760 nm O_2-A band using the *in-filling* method based on the Fraunhofer Line Depth principle (FLD) calculated from a total of three spectral bands (FLD3) as follows,

$$SIF = \frac{E_{out}\, L_{in} - E_{in}\, L_{out}}{E_{out}\, E_{in}} \quad (2)$$

where radiance, L, corresponds to L_{in} (L_{761}), L_{out} (average of L_{747} and L_{780} bands), and the irradiance, E, to E_{in} (E_{761}), and E_{out} (average of E_{747} and E_{780} bands). Values of SIF were rescaled through addition of an offset value to ensure that calculations of SIF from Eq. 2 were not negative.

2.3. Photosynthetic capacity

Measurements of photosynthetic capacity were made using a coupled chlorophyll fluorescence and gas-exchange system (Imaging-PAM M-Series and GFS-3000, Walz, Effeltrich, Germany) from the 7th to 16th of October 2019 following measurements of hyperspectral data. For each of the 30 plants, the response of assimilation to intercellular CO_2 concentration (A/C_i response) was measured on two to three fully expanded young fascicles that were selected from the upper third of the canopy. These needles were arranged inside the 6 cm^2 cuvette without overlap and the area for these needles was determined by differentiating thresholded pixels using the Imaging-Win software of the coupled system. During the course of the measurements, conditions in the cuvette were maintained at 20 °C, with a relative humidity of 60% and an irradiance of 1000 μmol photons m^{-2} s^{-1}. The external CO_2 concentration (C_a) supplied to the plants included the following series: 400, 300, 200, 100, 75, 50, 400, 600, 800, 1000, 1200, 1500, 2000 μmol mol^{-1}. Measurements were recorded after values of A, C_i and g_s were stable.

A/C_i curves were analysed using Farquhar-type equations (Long and Bernacchi, 2003). A generalised nonlinear least squares regression (*gnls* function, nlme package in R) was used to estimate V_{cmax} and J_{max}.

2.4. Determination of foliage N, P and chlorophyll

Following the completion of the A/C_i response curves, approximately 10 fully extended fascicles, were selected from the upper third of the crown of each plant. These fascicles were dried at 70 °C for at least 48 h to constant dry mass and transported to the Landcare Research laboratory (Palmerston North, New Zealand) for analysis of N and P. Foliage samples were finely ground, acid digested by the Kjeldahl method, and the N and P concentrations were determined colorimetrically (Blakemore et al., 1987). Approximately 20 fully extended fascicles were selected for measurements of chlorophyll $a + b$ (Chl_{a+b}). These needles were placed in tubes and frozen at −80 °C before being transported with dry ice to Plant and Food Laboratory (Lincoln, New

Zealand) where analysis was undertaken using Chl_{a+b} estimation by spectrometry. From finely ground foliage samples, plant materials were extracted with acetone. This extraction was undertaken in the dark and the samples were kept on ice throughout the process to avoid pigment degradation. The absorbance of the extracts in the wavelengths 645, 652, 663, and 700 nm were read against 80% acetone and these values were then used to compute the chlorophyll concentration (Holden, 1965). All values of chlorophyll reported here refer to the total chlorophyll (Chl_{a+b}).

Specific leaf area, (SLA) was determined from needles sampled for chlorophyll and expressed on a hemisurface leaf area basis. Following Bown et al. (2009b) leaf area was determined from $[nld(1 + \pi/n)]/2$, where d is fascicle diameter, l is fascicle length and n is the number of needles per fascicle. SLA was expressed in μg cm^{-2} as the quotient of dry weight and leaf area. Measurements of SLA were used to convert foliage nutrient and pigment concentrations to a hemisurface area basis.

2.5. Measurements of tree dimensions

Tree height, root collar diameter and crown diameter were measured on the 22nd October 2019. Crown diameter was measured in two perpendicular directions at the widest point and these measurements were averaged. Electronic calipers were used to measure root collar diameter and both height and crown width were measured using a tape.

2.6. Data analysis

All analyses were undertaken at the plant level using a combination of Matlab (The MathWorks, Inc., Natick, Massachusetts, United States) and R (R Development Core Team, 2011). Matlab was used to plot the spectra and invert PROSAIL while all other analyses were undertaken using R.

2.6.1. Treatment differences

Tree dimensions, foliage nutrient content, photosynthetic variables, and PROSAIL output were tabulated and one-way analysis of variance was used to test for treatment differences between these variables. Multiple range testing, using the Tukey test, was used to determine which treatments significantly differed for all variables in which treatment had a significant effect.

Treatment variation in hyperspectral variables was plotted. We undertook a one-way analysis of variance across each of the 396 reflectance bands to identify which bands were most sensitive to the treatments. This band level ANOVA was also undertaken on four different treatment contrasts to isolate the influence of N and P on reflectance. The influence of N was determined through contrasting reflectance for low and high N treatments at both low (N0P0 vs N1P0) and high P (N0P1 vs. N1P1). Similarly, the influence of P on reflectance was identified through contrasting low and high P treatments at both low (N0P0 vs N0P1) and high N (N1P0 vs. N1P1). Using a Bonferroni correction these contrasts were deemed to be significant at $P < .0125$.

2.6.2. Prediction of photosynthetic variables

Nutrient ratios were used to separate the dataset into plants that were either N or P limiting to gain greater insight into the processes regulating photosynthetic capacity within each of these two phases. Following previous literature (Aerts and Chapin, 2000; Knecht and Göransonn, 2004; Marschner, 1995; Reich and Schoettle, 1988) trees with an N:P ratio (expressed on a mass basis) of ≤10 were categorised as N deficient, while those with N:P > 10 were categorised as P deficient. The foliage N:P within sampled trees ranged from 2.6–27.9, of which 9 observations were P limited while the remaining 21 were N limited (Fig. 2).

Following Kattenborn et al. (2019) all modelling used nutrient concentrations expressed on an area basis. Initial analyses examined correlations between N, P, and PRI and SIF. Bivariate relationships were then developed between the photosynthetic variables and N, P, Chl_{a+b} to examine the role that these variables played in regulating photosynthetic capacity. The potential of predicting V_{cmax} and J_{max} from hyperspectral data was then investigated through development of models that included either $Chl_{a+b\ PROSAIL}$, PRI or SIF. In all developed models only significant variables were included in the models and variables were used in the models in either linear formulations, and where significant, in a polynomial formulation.

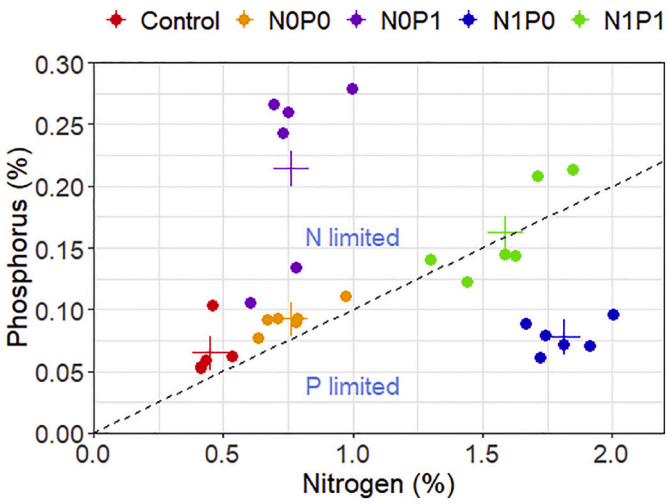

Fig. 2. Relationships between mass based nitrogen and phosphorus. The treatment designation for individual trees are denoted by filled circles while treatment means are shown as large crosses with differing colours. The dashed line represents a N:P ratio of 10. Values of foliage N and P content above the line are N limited while those below the line are P limited.

3. Results

3.1. Tree characteristics

All physical dimensions varied significantly between treatments (Appendix 1) and dimensions for the two high N treatments were markedly greater than those for the three low N treatments. Mean height, root collar diameter and crown width in N1P1 were, respectively, 85.8 cm, 15.9 mm and 31.6 cm, which exceeded corresponding mean values for these three dimensions in the Control, N0P1 and N0P1, by respectively, 58, 31 and 64%. There were no significant treatment differences in SLA and values averaged 2467 μg cm^{-2} across treatments (Appendix 1).

3.2. Foliar nutrition

The applied treatments resulted in a wide range in N and P (Fig. 2) and both elements significantly varied between treatments when expressed on either a mass or area basis (Appendix 1). Values of N ranged from 0.41–2.00% when expressed on a mass basis and 11.1–45.8 μg cm^{-2} on an area basis while P varied from respectively 0.053–0.278% and 1.41–6.47 μg cm^{-2}. The relationship between N and P was weakly significant (Fig. 2) when data was expressed on a mass basis ($P = .03$; $R^2 = 0.224$) but insignificant when expressed on an area basis ($P = .10$; $R^2 = 0.155$). The relationship between N and Chl_{a+b} was positive, highly significant and very strong when expressed on either a mass ($P < .001$; $R^2 = 0.887$) or area basis ($P < .001$; $R^2 = 0.870$).

When expressed on an area basis there were no significant differences in N or Chl_{a+b} (Appendix 1) between the two high N treatments (N1P0, N1P1) or the two low N treatments (N0P0, N0P1). Similarly, P

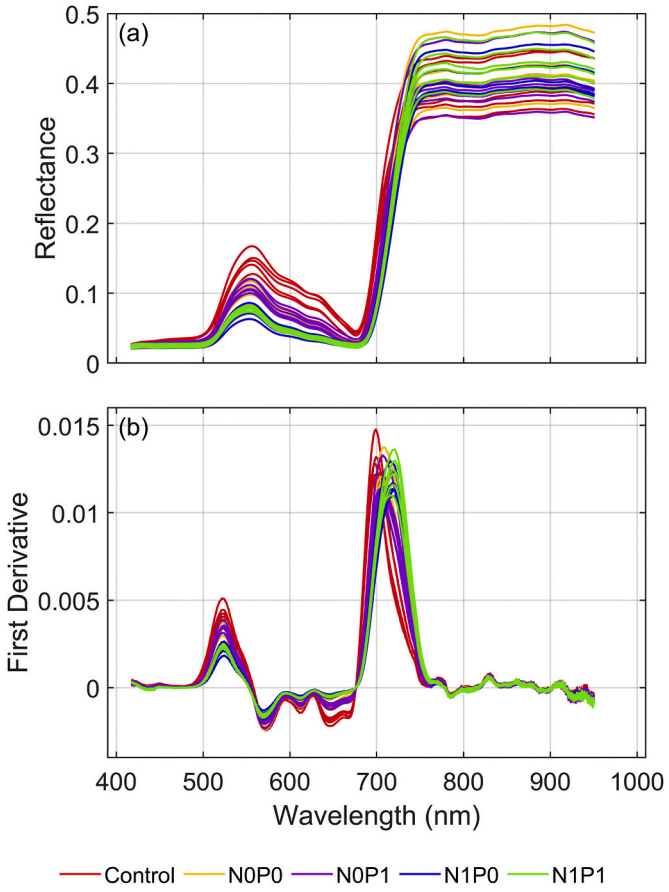

Fig. 3. Tree level variation in (a) canopy reflectance and (b) the 1st derivative of canopy reflectance against wavelength. Treatment identity is denoted by lines with differing colours.

did not significantly differ between the two low P treatments (N0P0, N1P0) or the two high P treatments (N0P1, N1P1). There was an identical significance pattern for N, P and Chl_{a+b} expressed on a mass basis (Appendix 1), except for the pairwise comparison of N for the two high N treatments (N1P0 and N1P1) which exhibited significant differences. This low level of lack of significance provided a sound basis for the pairwise testing of the impacts of N and P on both photosynthetic capacity and hyperspectral imagery, that is described below.

3.3. Photosynthesis capacity

Differences between treatments were highly significant for both V_{cmax} and J_{max} ($P < .001$). The mean values of V_{cmax} and J_{max} for N1P1, were respectively, 34.9 and 90.5 μmol m^{-2} s^{-1} which exceeded those in the Control treatment by ca. three-fold for both variables (Appendix 1). Most variation between the treatments was attributable to addition of N (Appendix 1). Values for the two high N treatments (N1P0, N1P1) significantly exceeded those of the two low N treatments, with equivalent P additions (N0P0, N0P1) by respectively 55 and 51% for V_{cmax} and J_{max} (Appendix 1). Addition of P to the low N treatment (i.e. N0P1 vs N0P0) increased V_{cmax} and J_{max} by respectively 7.8 and 3.3%, while addition of P to the high N treatment (i.e. N1P1 vs N1P0) resulted in greater increases to V_{cmax} and J_{max} of respectively, 11.5 and 16.2% (Appendix 1).

3.4. Hyperspectral data

Fig. 3 shows variation in canopy reflectance and the 1st derivative of reflectance at the tree level while Fig. 4 describes variation in reflectance across the entire spectrum and within three narrow wavelength ranges for data averaged by treatment (Fig. 4 a – d) and type of limitation (Fig. 4e – h). Tree level variation in reflectance was relatively tightly clustered within treatments highlighting the consistency of the data (Fig. 3a). Treatment level reflectance was higher in the low N treatments between 450 and 680 nm with the highest values recorded in the Control treatment (4a – d). There was also a marked shift in the lower wavelengths of the red edge for the low N treatments compared to those with high N (Fig. 4d). Both of these treatment influences on reflectance were significant, with the highest levels of significance occurring at wavelengths centred in the red edge at 700 nm and the green peak at 580 nm (Fig. 5), with significant treatment differences occurring at all other wavelengths between 472 and 728 nm (Fig. 5).

The first derivative of reflectance for the three low N treatments exhibited marked increases between 500 and 550 nm (Fig. 3b), compared to the two high N treatments and peak values for the first derivative were reached at lower wavelengths, with both features being most marked for the Control treatment (Fig. 3b). Significant treatment differences were noted in the first derivative in almost all wavelengths between 422 and 811 nm with the most significant differences occurring at wavelengths centred around 497 and 647 nm (Fig. 5).

Analysis of variance, using treatment combinations that partitioned the impact of N and P, showed that treatment differences were mainly attributable to variation in N. For reflectance, comparisons of low and high P at similar values of N, that were either low (i.e. N0P0 vs. N0P1, red circles, Fig. 6a) or high (i.e. N1P0 vs. N1P1, blue circles, Fig. 6a) did not significantly differ. The small influence of P on reflectance is also clearly evident in figures showing spectral changes across discrete ranges which shows these two P contrasts almost overlap between 400

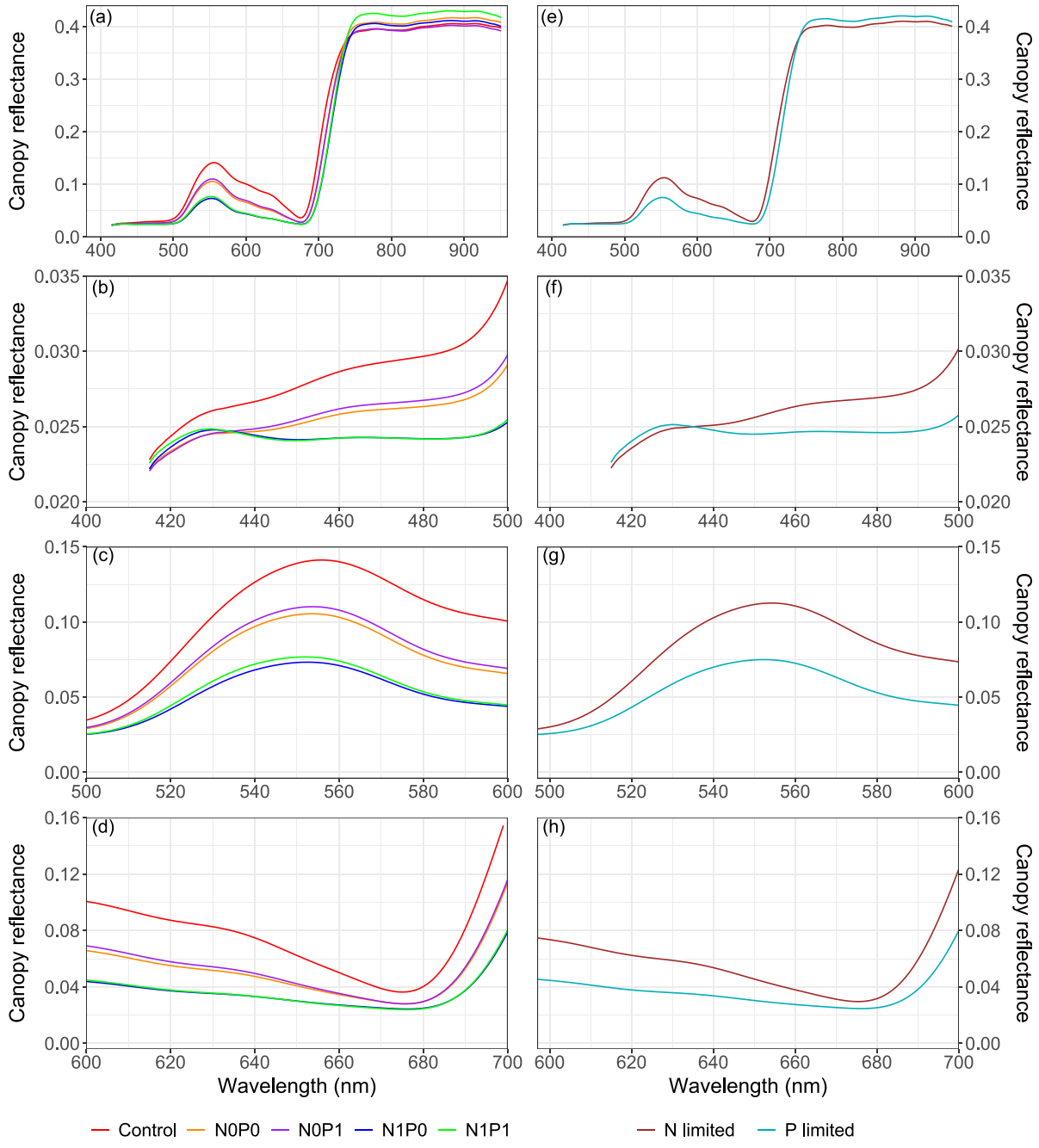

Fig. 4. Variation in (a, e) canopy reflectance across the entire spectrum and between (b, f) 400–500 nm, (c, g) 500–600 nm and (d, h) 600–700 nm for data averaged by (a – d) treatment and (e – h) limitation type.

and 700 nm (Figs. 4b–d). Similarly, for the first derivative, these two treatment comparisons were mostly non-significant, with the exception of a few wavelengths, scattered across the spectral range (Fig. 6b).

In contrast, comparisons of reflectance for low and high N, made at low values of P (green circles, Fig. 6a) or high values of P (black circles, Fig. 6a) showed significant differences between treatments from ca. 500–730 nm, reaching highest significance for both comparisons in the red edge region, and at wavelengths centred around 534 nm for N0P1 vs. N1P1 (Fig. 6a). Treatment contrasts shown for discrete spectral regions (Figs. 4b–d) show that higher N markedly reduces reflectance, compared to low N, for both contrasts and that these differences are particularly marked within the green peak region (Fig. 4c).

Treatment comparisons were in general more significantly different for the first derivative of reflectance than reflectance (Fig. 6b). Differences in the first derivative for these two N treatment comparisons were significant across most of the spectral range, from ca. 432–763 nm, with the most significant values occurring in the red-edge region for N0P0 vs. N1P0 and at wavelengths centred around 504, 608 and 651 nm for N0P1 vs. N1P1 (Fig. 6b).

When expressed by the type of limitation, trees that were limited by N had higher reflectance than P limited trees within both the red edge range and visible spectrum above 430 nm (Fig. 4e). These differences were most marked within the green peak region (Fig. 4g). There was also a marked shift in the lower wavelengths of the red edge for the N limited plants compared to those that were P limited (Fig. 4h).

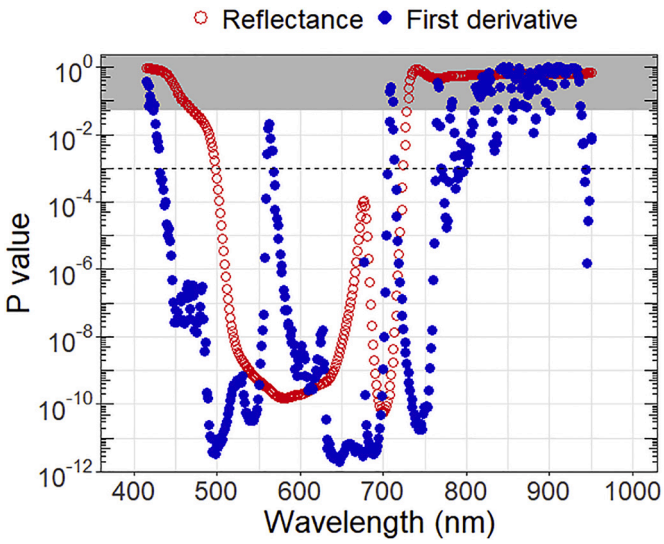

Fig. 5. Variation in treatment significance, as indicated by the *P*-value, for reflectance (open red circles) and the first derivative of reflectance (filled blue circles). The grey region shown at the top of the figure outlines the area of insignificance at $P > .05$ while the dashed line is drawn at $P = .001$. The y-axis is shown as a logarithmic scale to highlight the significance strength. (For interpretation of the references to colour in this figure legend, the reader is referred to the web version of this article.)

3.5. Relationships between nutrient content and spectral indices

Within the N limiting range there were significant positive relationships between N and both PRI ($P < .001$; $R^2 = 0.83$; Fig. 7a) and SIF ($P < .001$; $R^2 = 0.59$; Fig. 7c) but relationships between N and both of these variables were insignificant and weak, within the P limiting range (Fig. 7a, c). In the P limiting range, strong significant positive relationships were found between P and both SIF ($P < .01$; $R^2 = 0.697$) and $PRI_{528,\ 567}$ ($P < .001$; $R^2 = 0.792$), as shown by the filled teal circles, respectively, in Figs. 7d and b. Within the N limiting range, the relationship between P and SIF was insignificant and weak ($P = .23$; $R^2 = 0.076$), while the relationship between P and $PRI_{528,\ 567}$ was only marginally significant but very weak ($P = .048$; $R^2 = 0.190$).

3.6. Models of photosynthetic capacity

3.6.1. Use of measured variables

Under both N and P limiting conditions Chl_{a+b} was most strongly related to both V_{cmax} ($P < .001$; $R^2 = 0.85$) and J_{max} ($P < .001$; $R^2 = 0.82$) and both relationships were positive (Fig. 8a, c; Table 2). There were strong positive relationships between N and both V_{cmax} ($P < .001$; $R^2 = 0.84$) and J_{max} ($P < .001$; $R^2 = 0.82$), that were only marginally weaker than the relationships with Chl_{a+b} (Fig. 9a, c; Table 2). Under N limiting conditions these relationships generally remained at similar strength, although N was a slightly stronger predictor of J_{max} than Chl_{a+b} ($R^2 = 0.87$ vs. 0.86). Under P limiting conditions, relationships between photosynthetic capacity and either N (Fig. 9 a, c) or Chl $_{a+b}$ (Fig. 8 a, c) were very weak ($R^2 < 0.02$) and insignificant (Table 2).

Under P limiting conditions, relationships between P and both V_{cmax} (Fig. 9b) and J_{max} (Fig. 9d) were positive, significant and of a moderate strength, with respective R^2 of 0.50 and 0.58 (Table 2). In contrast, relationships between P and photosynthetic capacity (V_{cmax}, J_{max}) were insignificant under either N limiting conditions or across the entire dataset (Figs. 9b, d; Table 2).

3.6.2. Use of derived variables

There was a strong linear relationship ($R^2 = 0.88$) between area based measured chlorophyll (C_{a+b}) and chlorophyll predicted by model inversion ($C_{a+b\ PROSAIL}$). Values of C_{a+b} were overpredicted by $C_{a+b\ PROSAIL}$ at low values and underpredicted at high values, but there was little treatment bias in the predictions (Fig. 10).

Using all the data, $Chl_{a+b\ PROSAIL}$ exhibited strong positive linear relationships (Fig. 8b, d) with both V_{cmax} ($P < .001$; $R^2 = 0.79$) and J_{max} ($P < .001$; $R^2 = 0.76$). These relationships remained significant and relatively strong using data restricted to N limiting conditions (Table 2). However, there was no significant relationship between $Chl_{a+b\ PROSAIL}$ and either both V_{cmax} and J_{max} under P limiting conditions, with $R^2 < 0.04$ for both relationships (Table 2; Fig. 8b, d).

Using all the data there were strong relationships between $PRI_{528,\ 567}$ and both V_{cmax} ($P < .001$; $R^2 = 0.84$) and J_{max} ($P < .001$; $R^2 = 0.84$) that were best described using quadratic terms (Table 2; Fig. 11a, c). These relationships remained strong, but the precision was slightly reduced when data was restricted to N limiting conditions (Table 2). Under P limiting conditions positive correlations of moderate strength were found between $PRI_{528,\ 567}$ and V_{cmax} ($P = .06$; $R^2 = 0.42$) and J_{max} ($P = .029$; $R^2 = 0.51$), that were generally aligned with predictions under N limiting conditions (Table 2; Fig. 11a, c).

Using all the data SIF exhibited strong positive linear relationships with both V_{cmax} ($P < .001$; $R^2 = 0.78$) and J_{max} ($P < .001$; $R^2 = 0.80$), which were slightly reduced in strength when data was restricted to N limiting measurements (Table 2; Fig. 11b, d). Under P limiting conditions, SIF was moderately related to V_{cmax} ($P = .09$; $R^2 = 0.35$) and strongly related to J_{max} ($P < .01$; $R^2 = 0.68$) and these relationships aligned very well with predictions made under N limiting conditions (Fig. 11b, d).

4. Discussion

Our results show that N and P were only significantly related to V_{cmax} and J_{max}, within the N and P limiting ranges, respectively,

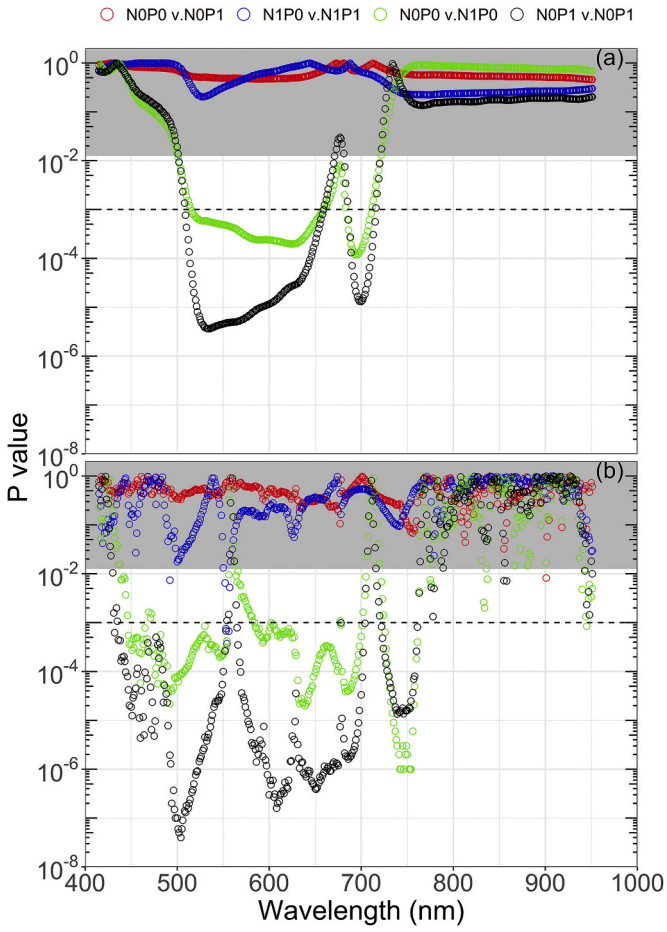

Fig. 6. Variation in treatment significance, as indicated by the *P*-value, for (a) reflectance and (b) the first derivative of reflectance, for comparisons of P under low (red circles) and high N (blue circles) and comparisons of N under low (green circles) and high P (black circles). The grey region shown at the top of the figure outlines the area of insignificance at $P > .0125$ while the dashed line is drawn at $P = .001$. The y-axis is shown as a logarithmic scale to highlight the significance strength. (For interpretation of the references to colour in this figure legend, the reader is referred to the web version of this article.)

suggesting that photosynthetic capacity is independently regulated by these elements. Predictions of photosynthetic capacity (V_{cmax}, J_{max}) using variables derived from hyperspectral imagery showed contrasting generality across the dataset. Strong positive relationships were observed between $Chl_{a+b\ PROSAIL}$ and both V_{cmax} and J_{max} in the N limiting phase but these relationships were insignificant in the P limiting range. However, both SIF and $PRI_{528,\ 567}$ exhibited moderate to strong positive relationships with photosynthetic capacity in both the N and P limiting phases suggesting that these variables are more generalisable than $Chl_{a+b\ PROSAIL}$.

The treatments used here created a wide range in N and P that exceeded the ranges in content and N:P ratio typically found in field grown *P. radiata*. When expressed on a mass basis foliage N ranged from 0.41 to 2.0% while foliage P ranged from 0.05 to 0.28%. Within a designed field experiment, located at 20 sites spanning almost all variation in soil fertility found in New Zealand plantations, ranges were markedly lower varying from 0.75–1.64% for N and from 0.09–0.18% for P (Watt et al., 2009). Our reported values in N and P covered ranges considered to be deficient, marginal and sufficient for both elements (Mead, 2013).

The use of ratios provided a useful means of separating N from P limitations. Nutrient ratios have been extensively used to identify optimum nutrition and account for particular nutrient limitations (Ingestad, 1971, 1979; Ingestad and Lund, 1986). In terrestrial plants an optimum N:P ratio of 10 has been found for a wide range of species (Knecht and Göransonn, 2004) which agrees with our results that show photosynthetic capacity peaks at ratios of 9.3–11.3 (data not shown). Several authors (Aerts and Chapin, 2000; Marschner, 1995; Reich and Schoettle, 1988) suggest that deviations from this N:P ratio of 10 should lead to nitrogen ($N:P \leq 10$) or phosphorus ($N:P > 10$) deficiencies. Our results strongly support this suggestion through showing that N and P were only significantly related to V_{cmax} and J_{max}, within the N and P limiting ranges, respectively.

Overall our results show that Chl_{a+b} and N had the largest influence on photosynthetic capacity. The strong relationships found here between photosynthetic capacity and both Chl_{a+b} and N under N limiting conditions have a sound physiological basis. Nitrogen is a major component of Rubisco (Niinemets and Tenhunen, 1997) and at least 50% of leaf nitrogen is invested in the photosynthetic apparatus of plants (Niinemets and Sack, 2006). As Rubisco catalyses the carboxylation reaction, there is a mechanistic link between the leaf Rubisco content and the maximum capacity of carboxylation, V_{cmax}.

Similarly, chlorophyll also plays an important role in photosynthesis. Chlorophyll which is embedded in the thykaloid membranes of

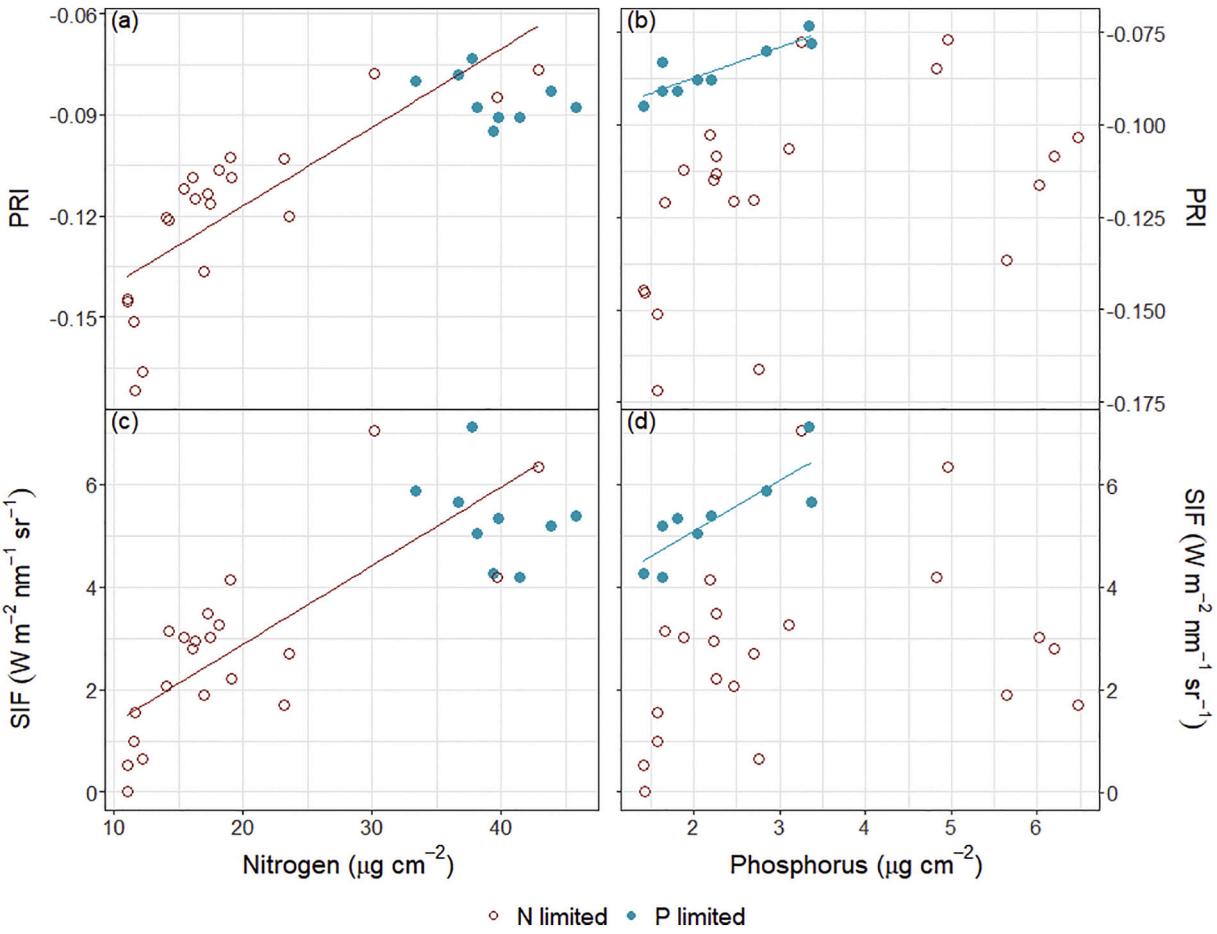

Fig. 7. Relationships between nitrogen and phosphorus content and (a, b) Photochemical Reflectance Index and (c, d) Sun Induced Chlorophyll Fluorescence, under N (open brown circles) and P limiting conditions (filled teal circles). Lines have been fitted to relationships that are significant at $P < .048$ with the brown and teal lines fitted respectively to N and P limited data. (For interpretation of the references to colour in this figure legend, the reader is referred to the web version of this article.)

chloroplasts, provides the principal means of harvesting light (Croft et al., 2017). This light harvest provides the energy to supply electrons, via the cytochrome b_6f complex, to produce nicotinamide adenine dinucleotide phosphate (NADPH) and chemical energy as adenosine triphosphate (ATP), for the reactions of the Calvin–Benson cycle. Chlorophyll content has been shown to be related to the amount of light harvested across a range of species (Collatz et al., 1991; Evans, 1996), and photosynthetically active radiation absorbed by the leaf drives the potential rate of electron transport, J (Collatz et al., 1991; Sellers et al., 1992). Although chlorophyll is theoretically more closely related to J_{max}, in practice a strong linear relationship between V_{cmax} and J_{max}, is often observed across a range of species (Medlyn et al., 2002) as was found for our data ($P < .001$; $R^2 = 0.939$). This tight coupling, which is thought to reflect coordination between these two rate-limiting biochemical cycles (Kattge and Knorr, 2007; Leuning, 1997; Medlyn et al., 2002; Walker et al., 2014), means that in practice Chl_{a+b} can be used as a predictor for both variables.

Under N limiting conditions, relationships between photosynthetic capacity and both Chl_{a+b} and N were found to have a very similar precision. This suggests that wavelengths associated with N in the SWIR range are not as important for predicting photosynthetic capacity in *P. radiata* as those associated with chlorophyll in the VNIR range. Examination of spectral differences between treatments confirm the importance of chlorophyll as a key predictor of photosynthetic capacity. These analyses show the most significant treatment differences occur within the green and red edge spectral regions which have previously been found to be key spectral predictors of chlorophyll content (Carter, 1994; Gitelson and Merzlyak, 1996; Horler et al., 1983; Rock et al., 1988; Vogelmann, 1993).

The significant positive relationships that we found between P and both V_{cmax} and J_{max} within the P limiting range were associated with high values of N. Results from a *P. radiata* nutrition experiment with a similar design (Bown et al., 2009a), that investigated relationships between nutrition and photosynthetic capacity, were very similar to ours and found a significant relationship between P and photosynthetic capacity in the P limiting range. This result is also consistent with a meta-study undertaken by Walker et al. (2014) who observed little gain in V_{cmax} and J_{max} under increasing P at low N, but a doubling of modelled gross carboxylation rates across a P range under high N levels, which is analogous to the P limiting range in our study. The importance of P in regulating V_{cmax} and J_{max} has a sound theoretical basis as the availability of P has an impact on many important aspects of photosynthesis including membrane solubility, ATP, and NADPH production (Marschner, 1995; Taiz et al., 2015).

Our results demonstrate very little spectral alteration associated with P but do show significant relationships between P and both PRI_{528},

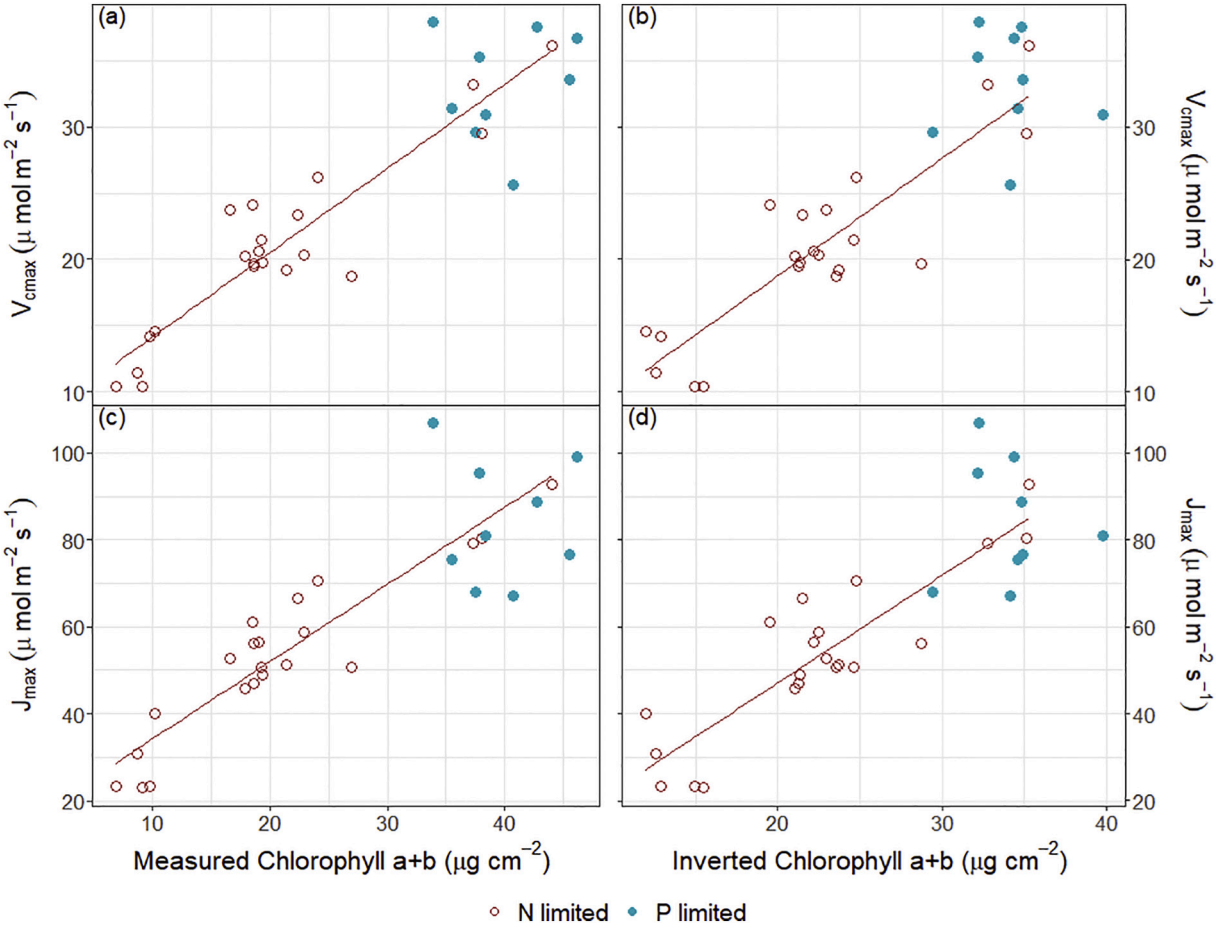

Fig. 8. Relationships between measured chlorophyll$_{a+b}$ and inverted chlorophyll$_{a+b}$ and (a, b) V_{cmax} and (c, d) J_{max} under N (open brown circles) and P limiting conditions (filled teal circles). Lines have been fitted to relationships that are significant at $P < .05$ with the brown lines fitted to N limited data. (For interpretation of the references to colour in this figure legend, the reader is referred to the web version of this article.)

Table 2
Summary of model precision, as denoted by the coefficient of determination (R^2) for models describing the maximal carboxylation capacity (V_{cmax}) and the maximal electron transport rate (J_{max}). Measured predictors include area based measurements of nitrogen (N), phosphorus (P) and chlorophyll (Chl$_{a+b}$). Predictors that were derived from hyperspectral data included Photochemical Reflectance Index (PRI), Sun-Induced Chlorophyll Fluorescence (SIF) and chlorophyll derived from the PROSAIL inversion (Chl$_{a+b\ PROSAIL}$).

Predictor(s)	All data		N limiting		P limiting	
	V_{cmax}	J_{max}	V_{cmax}	J_{max}	V_{cmax}	J_{max}
Measured variables						
N	0.84***	0.82***	0.82***	0.87***	0.01^{ns}	0.02^{ns}
P	0.04^{ns}	0.06^{ns}	0.33^{ns}	0.31^{ns}	0.50*	0.58*
Chl$_{a+b}$	0.85***	0.82***	0.85***	0.86***	0.02^{ns}	0.01^{ns}
Derived predictors						
Chl$_{a+b\ PROSAIL}$	0.79***	0.76***	0.64***	0.63***	0.03^{ns}	0.04^{ns}
SIF	0.78***	0.80***	0.69***	0.70***	0.35^{ns}	0.68**
PRI	0.84***	0.84***	0.73***	0.75***	0.42^{ns}	0.51*

$_{567}$ and SIF within the P limiting range. After controlling for N, results clearly show little discernible change in reflectance or the first derivative of reflectance between plants with high or low P. This is consistent with previous literature as P does not directly absorb energy in the shortwave spectrum and consequently predictions of P typically rely on strong positive correlations with N (Asner and Martin, 2008; Gillon et al., 1999; Porder et al., 2005). While this is a useful approach for vegetation with normal ratios of N and P, this empirical relationship is likely to break down when ratios of N and P deviate from normal values, and there is little correlation between N and P. Within the P limiting range there were moderate to strong positive, linear relationships between P and both SIF and PRI suggesting that these variables may act as proxies for P and the effect of this element on photosynthetic capacity.

Although the three variables, derived from the hyperspectral data, used to predict photosynthetic capacity had similar precision, there were marked differences in their utility for predicting photosynthetic capacity. The significant relationship found here between Chl$_{a+b\ PROSAIL}$ and photosynthetic capacity is consistent with previous research that has used chlorophyll derived from physically based models to predict V_{cmax} and J_{max} (Croft et al., 2017; Dechant et al., 2017). Our results generally support Croft et al. (2017), who advocate the use of chlorophyll as a potentially useful proxy for photosynthetic capacity but extend these findings through showing that chlorophyll should be used with caution under P limiting conditions, where we found this relationship to be weak and insignificant.

SIF was strongly correlated with both V_{cmax} and J_{max} and, in contrast to Chl$_{a+b\ PROSAIL}$, predictions exhibited relatively robust

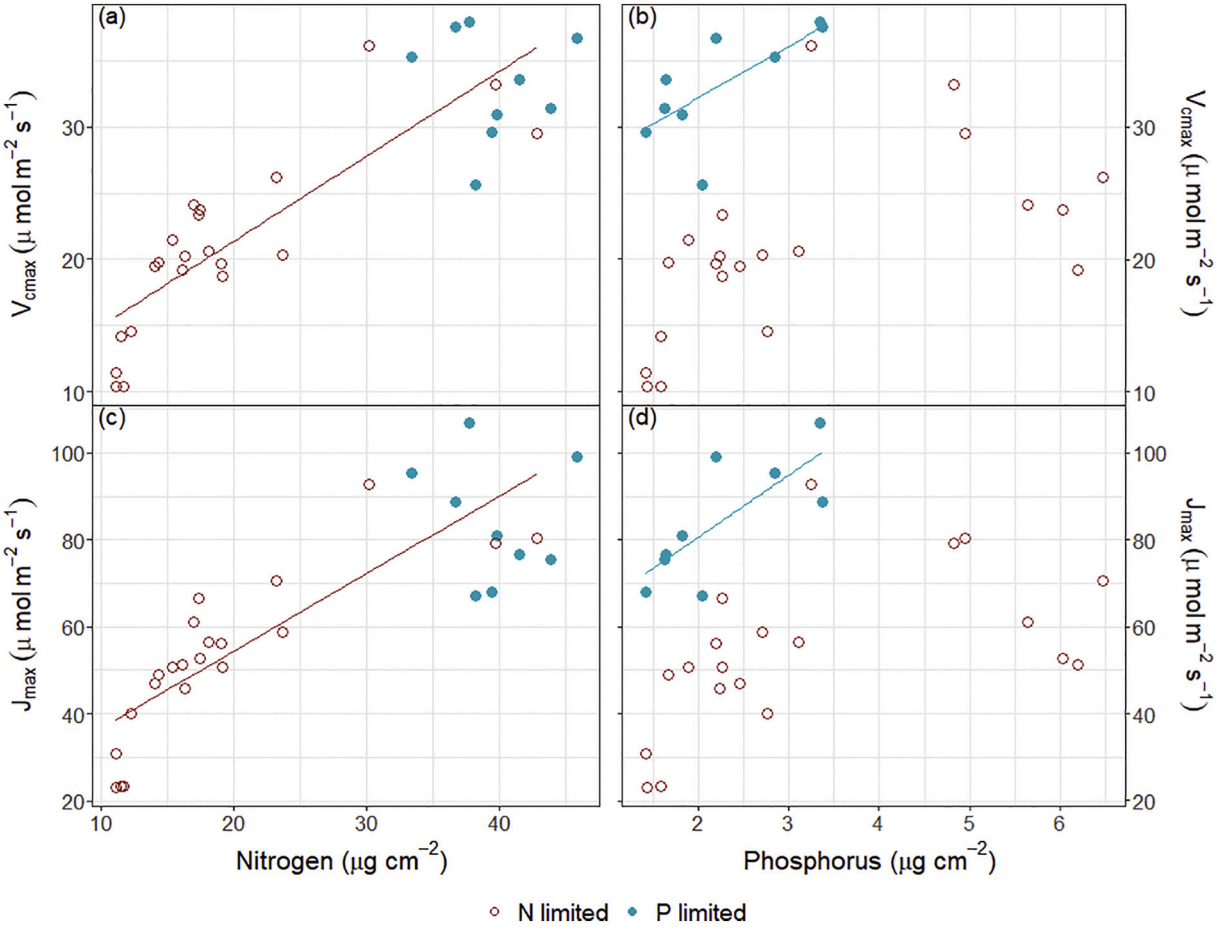

Fig. 9. Relationships between area based nitrogen and phosphorus and (a, b) V_{cmax} and (c, d) J_{max} under N (open brown circles) and P limiting conditions (filled teal circles). Lines have been fitted to relationships that are significant at $P < .05$ with the brown and teal lines fitted respectively to N and P limited data. (For interpretation of the references to colour in this figure legend, the reader is referred to the web version of this article.)

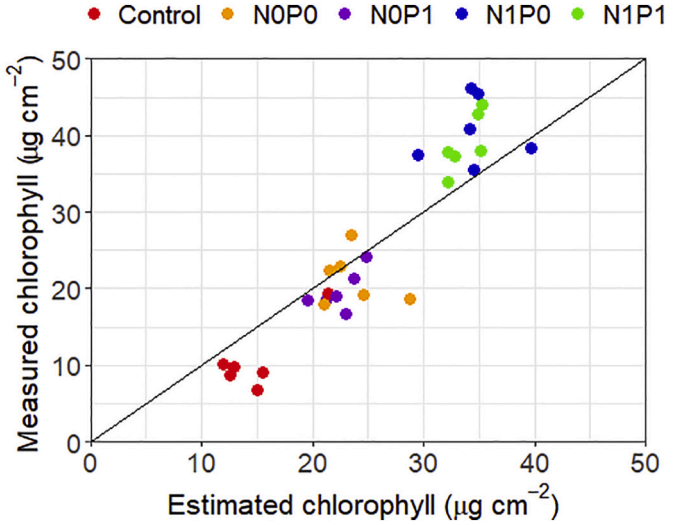

Fig. 10. Relationship between measured chlorophyll and estimated chlorophyll derived from the PROSAIL inversion. The 1:1 line is shown as a solid line and treatments are denoted by filled circles with differing colours.

correlations across both the N and P limiting ranges. Although SIF has been widely used to predict gross primary productivity (Meroni et al., 2009; Porcar-Castell et al., 2014; Rascher et al., 2015), and photosynthesis (Frankenberg et al., 2011; Guanter et al., 2014; Smith et al., 2018), in a range of species, with few exceptions (Camino et al., 2019) little research has linked SIF to V_{cmax} and J_{max} at a fine scale. As found here, there is generally a strong relationship between chlorophyll and SIF as leaves with a higher chlorophyll will absorb more light and produce a higher leaf SIF, although this effect is complicated by the fact that emitted SIF is scattered and reabsorbed throughout the canopy (Verrelst et al., 2015). It has been hypothesised that SIF is a useful predictor of photosynthetic capacity as it can be used to selectively measure the quantity of absorbed light in chlorophyll (Rascher et al., 2015). However, in contrast to Chl_{a+b}, our results suggest that SIF can at least partially account for the role of P on photosynthetic capacity at high values of N as supported by the strong relationship found between SIF and P under P limiting conditions.

Similarly, PRI was also strongly related to photosynthetic capacity and was able to account for variation in V_{cmax} and J_{max} across both N and P limitations. Research has widely demonstrated the utility of PRI for predicting light use efficiency (Garbulsky et al., 2011; Peñuelas et al., 2011) and key photosynthetic parameters under a range of stresses including severe drought conditions (Ripullone et al., 2011), cold winter temperatures (Gamon et al., 2016; Wong and Gamon, 2015a, 2015b) and herbicide damage (Scholten et al., 2019). The relationship found here between PRI and photosynthetic capacity is consistent with Scholten et al. (2019) and has a strong theoretical basis as PRI can track plant photosynthetic activity through its intimate link with the dissipation of excess energy by nonphotochemical quenching (NPQ) via the xanthophyll cycle. The xanthophyll cycle is activated during periods of excess excitation energy in the leaf and through this process violaxanthin is de-epoxidized to zeaxanthin. These increased concentrations in zeaxanthin reduce reflectance at wavelengths around

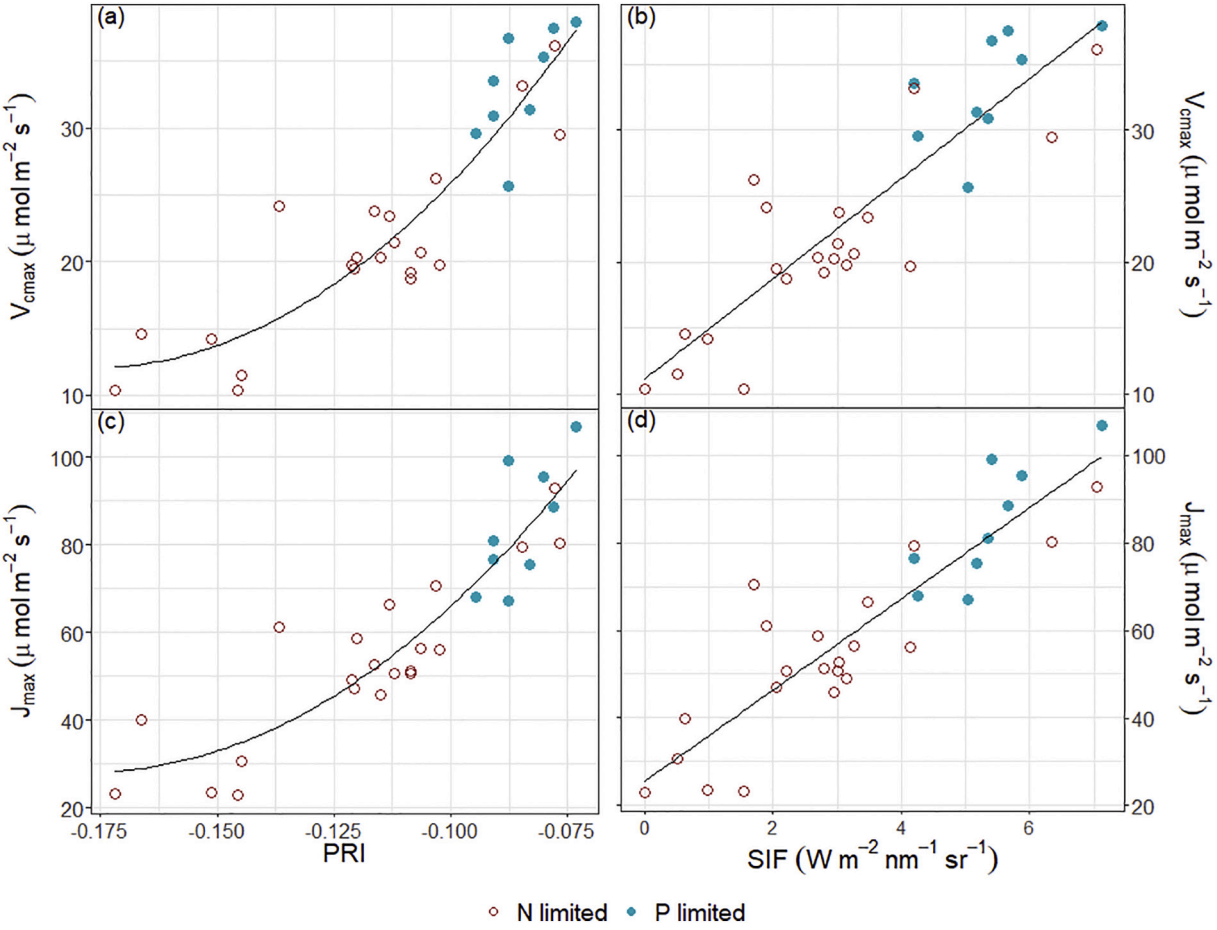

Fig. 11. Relationships between Photochemical Reflectance Index and Sun Induced Chlorophyll Fluorescence and (a, b) V_{cmax} and (c, d) J_{max} under N (open brown circles) and P limiting conditions (filled teal circles). The black lines were fitted to the combined N and P limited dataset. (For interpretation of the references to colour in this figure legend, the reader is referred to the web version of this article.)

531 nm, which results in reductions in PRI. Nevertheless, PRI has been demonstrated to be related to the absorption of chlorophyll content, in addition to the xanthophyll pigments, as well as by the canopy structure and soil (Suárez et al., 2009; Suárez et al., 2008; Zarco-Tejada et al., 2013b). Results found in this experiment show the potential contribution of both xanthophylls and chlorophyll in the observed relationships with photosynthetic capacity. As with SIF, our results suggest that PRI may provide a more generalisable means of predicting photosynthetic capacity under a range of nutritional limitations than chlorophyll derived from physically based models.

Predictions of photosynthetic capacity estimated by PRI and SIF could be scaled up using satellite imagery. As summarised in Mohammed et al. (2019) measurements of SIF are currently taken from a number of satellite platforms (e.g. GOME-2, OCO-2) and the first satellite mission designed for SIF measurement, FLEX, is scheduled for launch in 2022. The recently launched PRISMA and DESIS hyperspectral imagers, and the EnMAP sensor, which is scheduled for launch in 2021, are particularly suitable for estimating PRI and will provide imagery at a spatial resolution of 30 m with a relatively fine spectral resolution of up to 6.5 nm within the VNIR range (Guanter et al., 2015). In addition, Sentinel-3 has been proposed for V_{cmax} estimation at global scales using radiative transfer models such as SCOPE (Prikaziuk and van der Tol, 2019).

In conclusion, results from this study clearly demonstrate the utility of SIF and PRI for prediction of photosynthetic capacity across both the N and P limiting ranges. Although results clearly highlight the importance of N and Chl_{a+b} as key predictors of photosynthetic capacity we also show that these relationships break down within the P limiting range. The use of a N:P ratio to separate N from P limitations provided insight into relationships that would have otherwise have been concealed. Further research should examine the utility of this approach for development of models that link nutrient content and hyperspectral data to photosynthesis at increased scale across a broader range of species.

Declaration of Competing Interest

The authors declare that they have no known competing financial interests or personal relationships that could have appeared to influence the work reported in this paper.

Acknowledgements

We are grateful to Kendra Newick who assisted with the preparation of the nutrient solutions. The project was partly funded through the Resilient Forests programme, which is funded through Scion SSIF as well as the Forest Grower's Levy Trust. Funding was also received from the National Institute for Forest Products Innovation (Project Number NIF073-1819), which comprised contributions from the Australian Government, Australasian Forestry Companies and South Australian and Tasmanian State Governments.

Appendix A. Treatment variation in tree characteristics, photosynthetic variables, foliage nutrition, and predictor variables derived from hyperspectral data. Values shown include the mean followed by the standard deviation. Values presented for the ANOVA include the *F*-value followed by the *P* category, in which asterisks *, **, represent significance at *P* = .001 and 0.01, respectively, ns = non-significant at *P* = .05. For all variables with significant treatment differences multiple range testing was undertaken using the Tukey test. Treatment values followed by the same letter were not significantly different at *P* = .05**

Variable	Control	N0P0	N0P1	N1P0	N1P1	ANOVA
Tree characteristics						
Height (cm)	54.2 (5.11)a	66.3 (7.07)a	63.2 (7.27)a	85.3 (19.8)b	85.8 (6.70)b	10.5***
Tree diam. (mm)	13.2 (1.88)a	12.9 (1.50)a	12.1 (1.45)a	14.7 (1.95)ab	15.9 (1.08)b	5.49**
Crown diam. (cm)	20.1 (3.70)a	22.4 (3.83)ab	19.2 (3.25)a	26.5 (3.33)bc	31.6 (2.36)c	14.3***
SLA (μg cm^{-2})	2858 (573)	2306 (518)	2406 (226)	2288 (234)	2478 (647)	1.44^{ns}
Photosynthetic variables						
V_{cmax} (μmol m^{-2} s^{-1})	13.5 (3.60)a	20.6 (1.61)b	22.2 (2.87)b	31.3 (3.73)c	34.9 (3.16)c	46.6***
J_{max} (μmol m^{-2} s^{-1})	31.6 (10.8)a	54.7 (7.31)b	56.5 (8.36)b	77.9 (11.7)c	90.5 (10.3)c	32.3***
Foliage nutrition – mass based						
N (%)	0.447 (0.045)a	0.758 (0.120)b	0.759 (0.131)b	1.81 (0.127)c	1.58 (0.194)d	119***
P (%)	0.065 (0.019)a	0.093 (0.011)ab	0.214 (0.075)c	0.078 (0.013)ab	0.162 (0.039)c	15.7***
Chl_{a+b} (%)	0.399 (0.165)a	0.878 (0.140)b	0.849 (0.113)b	1.78 (0.192)c	1.68 (0.162)c	85.3***
Foliage nutrition – area based						
N (μg cm^{-2})	12.0 (1.21)a	18.4 (2.93)b	17.6 (3.05)b	41.4 (2.91)c	36.7 (4.50)c	105***
P (μg cm^{-2})	1.74 (0.51)a	2.26 (0.26)a	4.98 (1.74)b	1.79 (0.29)a	3.76 (0.89)b	14.3***
Chl_{a+b} (μg cm^{-2})	10.7 (4.42)a	21.4 (3.41)b	19.7 (2.63)b	40.6 (4.39)c	39.0 (3.76)c	71.2***
Derived predictor traits						
Inverted Chl_{ab} (μg cm^{-2})	14.9 (3.47)a	23.7 (2.82)b	22.4 (1.86)b	34.5 (3.27)c	33.7 (1.51)c	56.6***
PRI	−0.150 (0.018)a	−0.112 (0.006)b	−0.115 (0.012)b	−0.089 (0.004)c	−0.078 (0.004)c	42.4***
SIF (W m^{-2} nm^{-2} sr^{-1})	1.14 (1.11)a	3.08 (0.67)ab	2.46 (0.65)b	4.90 (0.54)c	6.04 (1.08)c	32.1***

References

Aerts, R., Chapin, F.S., 2000. The mineral nutrition of wild plants revisited: a re-evaluation of processes and patterns. Adv. Ecol. Res. 30, 1–67.

Asner, G.P., Martin, R.E., 2008. Spectral and chemical analysis of tropical forests: scaling from leaf to canopy levels. Remote Sens. Environ. 112, 3958–3970.

Asner, G.P., Martin, R.E., Knapp, D.E., Tupayachi, R., Anderson, C., Carranza, L., Martinez, P., Houcheime, M., Sinca, F., Weiss, P., 2011a. Spectroscopy of canopy chemicals in humid tropical forests. Remote Sens. Environ. 115, 3587–3598.

Asner, G.P., Martin, R.E., Tupayachi, R., Emerson, R., Martinez, P., Sinca, F., Powell, G.V.N., Wright, S.J., Lugo, A.E., 2011b. Taxonomy and remote sensing of leaf mass per area (LMA) in humid tropical forests. Ecol. Appl. 21, 85–98.

Beer, C., Reichstein, M., Tomelleri, E., Ciais, P., Jung, M., Carvalhais, N., Rödenbeck, C., Arain, M.A., Baldocchi, D., Bonan, G.B., 2010. Terrestrial gross carbon dioxide uptake: global distribution and covariation with climate. Science 329, 834–838.

Berger, K., Atzberger, C., Danner, M., D'Urso, G., Mauser, W., Vuolo, F., Hank, T., 2018. Evaluation of the PROSAIL model capabilities for future hyperspectral model environments: a review study. Remote Sens. 10, 85.

Blakemore, L.C., Searl, P.L., Daly, B.K., 1987. Methods for chemical analysis of soils. NZ Soil Bureau Sci. Rep. 80, 21–45.

Bown, H.E., Watt, M.S., Clinton, P.W., Mason, E.G., Richardson, B., 2007. Partitioning concurrent influences of nitrogen and phosphorus supply on photosynthetic model parameters of Pinus radiata. Tree Physiol. 27, 335–344.

Bown, H.E., Mason, E.G., Clinton, P.W., Watt, M.S., 2009a. Chlorophyll fluorescence response of Pinus radiata clones to nitrogen and phosphorus supply. Ciencia E Investig. Agraria 36, 451–464.

Bown, H.E., Watt, M.S., Mason, E.G., Clinton, P.W., Whitehead, D., 2009b. The influence of nitrogen and phosphorus supply and genotype on mesophyll conductance limitations to photosynthesis in *Pinus radiata*. Tree Physiol. 29, 1143–1151.

Buddenbaum, H., Pueschel, P., Stellmes, M., Werner, W., Hill, J., 2011. Measuring water and chlorophyll content on the leaf and canopy scale. EARSeL eProc. 10, 66–72.

Buddenbaum, H., Stern, O., Paschmionka, B., Hass, E., Gattung, T., Stoffels, J., Hill, J., Werner, W., 2015. Using VNIR and SWIR field imaging spectroscopy for drought stress monitoring of beech seedlings. Int. J. Remote Sens. 36, 4590–4605.

Buddenbaum, H., Watt, M.S., Scholten, R.C., Hill, J., 2019. Preprocessing ground-based visible/near infrared imaging spectroscopy data affected by smile effects. Sensors 19, 1543.

Camino, C., Gonzalez-Dugo, V., Hernandez, P., Zarco-Tejada, P.J., 2019. Radiative transfer Vcmax estimation from hyperspectral imagery and SIF retrievals to assess photosynthetic performance in rainfed and irrigated plant phenotyping trials. Remote Sens. Environ., 111186.

Carter, G.A., 1994. Ratios of leaf reflectances in narrow wavebands as indicators of plant stress. Remote Sens. 15, 697–703.

Cendrero-Mateo, M.P., Moran, M.S., Papuga, S.A., Thorp, K.R., Alonso, L., Moreno, J., Ponce-Campos, G., Rascher, U., Wang, G., 2015. Plant chlorophyll fluorescence: active and passive measurements at canopy and leaf scales with different nitrogen treatments. J. Exp. Bot. 67, 275–286.

Chen, J.M., Leblanc, S.G., Cihlar, J.C., Bicheron, P., Leroy, M., Deering, D., Eck, T., 1997. Studies of BRDF in Conifer and Deciduous Boreal Forests Using the 4-Scale Model and Airborne POLDER and Ground-Based PARABOLA Measurements. IEEE, pp. 165–167.

Collatz, G.J., Ball, J.T., Grivet, C., Berry, J.A., 1991. Physiological and environmental regulation of stomatal conductance, photosynthesis and transpiration: a model that includes a laminar boundary layer. Agric. For. Meteorol. 54, 107–136.

Colombo, R., Meroni, M., Marchesi, A., Busetto, L., Rossini, M., Giardino, C., Panigada, C., 2008. Estimation of leaf and canopy water content in poplar plantations by means of hyperspectral indices and inverse modeling. Remote Sens. Environ. 112, 1820–1834.

Croft, H., Chen, J., Zhang, Y., 2014. The applicability of empirical vegetation indices for determining leaf chlorophyll content over different leaf and canopy structures. Ecol. Complex. 17, 119–130.

Croft, H., Chen, J.M., Luo, X., Bartlett, P., Chen, B., Staebler, R.M., 2017. Leaf chlorophyll content as a proxy for leaf photosynthetic capacity. Glob. Chang. Biol. 23, 3513–3524.

Curran, P.J., Dungan, J.L., Peterson, D.L., 2001. Estimating the foliar biochemical concentration of leaves with reflectance spectrometry: testing the Kokaly and Clark methodologies. Remote Sens. Environ. 76, 349–359.

Dechant, B., Cuntz, M., Vohland, M., Schulz, E., Doktor, D., 2017. Estimation of photosynthesis traits from leaf reflectance spectra: correlation to nitrogen content as the dominant mechanism. Remote Sens. Environ. 196, 279–292.

Dobrowski, S.Z., Pushnik, J.C., Zarco-Tejada, P.J., Ustin, S.L., 2005. Simple reflectance indices track heat and water stress-induced changes in steady-state chlorophyll fluorescence at the canopy scale. Remote Sens. Environ. 97, 403–414.

Domingues, T.F., Meir, P., Feldpausch, T.R., Saiz, G., Veenendaal, E.M., Schrodt, F., Bird, M., Djagbletey, G., Hien, F., Compaore, H., 2010. Co-limitation of photosynthetic capacity by nitrogen and phosphorus in West Africa woodlands. Plant Cell Environ. 33, 959–980.

Doughty, C.E., Asner, G.P., Martin, R.E., 2011. Predicting tropical plant physiology from leaf and canopy spectroscopy. Oecologia 165, 289–299.

Drolet, G.G., Middleton, E.M., Huemmrich, K.F., Hall, F.G., Amiro, B.D., Barr, A.G., Black, T.A., McCaughey, J.H., Margolis, H.A., 2008. Regional mapping of gross light-use efficiency using MODIS spectral indices. Remote Sens. Environ. 112, 3064–3078.

Evans, J.R., 1996. Developmental constraints on photosynthesis: effects of light and nutrition. Photosynth. Environ. 281–304 (Springer).

Fang, M., Ju, W., Zhan, W., Cheng, T., Qiu, F., Wang, J., 2017. A new spectral similarity water index for the estimation of leaf water content from hyperspectral data of leaves. Remote Sens. Environ. 196, 13–27.

Farquhar, G.D., von Caemmerer, S., Berry, J.A., 1980. A biochemical model of photosynthetic CO_2 assimilation in leaves of C_3 species. Planta 149, 78–90.

Féret, J.B., Gitelson, A.A., Noble, S.D., Jacquemoud, S., 2017. PROSPECT-D: towards modeling leaf optical properties through a complete lifecycle. Remote Sens. Environ. 193, 204–215.

Frankenberg, C., Butz, A., Toon, G.C., 2011. Disentangling chlorophyll fluorescence from atmospheric scattering effects in O2 A-band spectra of reflected sun-light. Geophys. Res. Lett. 38.

Fuentes, D.A., Gamon, J.A., Cheng, Y., Claudio, H.C., Qiu, H.-l., Mao, Z., Sims, D.A., Rahman, A.F., Oechel, W., Luo, H., 2006. Mapping carbon and water vapor fluxes in a

chaparral ecosystem using vegetation indices derived from AVIRIS. Remote Sens. Environ. 103, 312–323.
Gamon, J., Penuelas, J., Field, C., 1992. A narrow-waveband spectral index that tracks diurnal changes in photosynthetic efficiency. Remote Sens. Environ. 41, 35–44.
Gamon, J., Serrano, L., Surfus, J.S., 1997. The photochemical reflectance index: an optical indicator of photosynthetic radiation use efficiency across species, functional types, and nutrient levels. Oecologia 112, 492–501.
Gamon, J.A., Filella, A., Penuelas, J., 1993. The dynamic 531-Nanometer Ä reflectance signal: A survey of twenty angiosperm species. In: Photosynthetic Responses to the Environment. American Society of Plant Physiologists, Rockville, MD USA, pp. 172–177.
Gamon, J.A., Huemmrich, K.F., Wong, C.Y.S., Ensminger, I., Garrity, S., Hollinger, D.Y., Noormets, A., Peñuelas, J., 2016. A remotely sensed pigment index reveals photosynthetic phenology in evergreen conifers. Proc. Natl. Acad. Sci. 113, 13087–13092.
Garbulsky, M.F., Peñuelas, J., Gamon, J., Inoue, Y., Filella, I., 2011. The photochemical reflectance index (PRI) and the remote sensing of leaf, canopy and ecosystem radiation use efficiencies: a review and meta-analysis. Remote Sens. Environ. 115, 281–297.
Gastellu-Etchegorry, J.-P., Demarez, V., Pinel, V., Zagolski, F., 1996. Modeling radiative transfer in heterogeneous 3-D vegetation canopies. Remote Sens. Environ. 58, 131–156.
Genty, B., Briantais, J., Baker, N.R., 1989. The relationship between the quantum yield of photosynthetic electron transport and quenching of chlorophyll fluorescence. Biochim. Biophys. Acta 990, 87–92.
Gillon, D., Houssard, C., Joffre, R., 1999. Using near-infrared reflectance spectroscopy to predict carbon, nitrogen and phosphorus content in heterogeneous plant material. Oecologia 118, 173–182.
Gitelson, A.A., Merzlyak, M.N., 1996. Signature analysis of leaf reflectance spectra: algorithm development for remote sensing of chlorophyll. J. Plant Physiol. 148, 494–500.
Gitelson, A.A., Kaufman, Y.J., Merzlyak, M.N., 1996. Use of a green channel in remote sensing of global vegetation from EOS-MODIS. Remote Sens. Environ. 58, 289–298.
Gitelson, A.A., Gamon, J.A., Solovchenko, A., 2017. Multiple drivers of seasonal change in PRI: implications for photosynthesis 1. Leaf level. Remote Sens. Environ. 191, 110–116.
Groenendijk, M., Dolman, A.J., Van der Molen, M.K., Leuning, R., Arneth, A., Delpierre, N., Gash, J.H.C., Lindroth, A., Richardson, A.D., Verbeeck, H., 2011. Assessing parameter variability in a photosynthesis model within and between plant functional types using global Fluxnet eddy covariance data. Agric. For. Meteorol. 151, 22–38.
Guanter, L., Zhang, Y., Jung, M., Joiner, J., Voigt, M., Berry, J.A., Frankenberg, C., Huete, A.R., Zarco-Tejada, P., Lee, J.-E., 2014. Global and time-resolved monitoring of crop photosynthesis with chlorophyll fluorescence. Proc. Natl. Acad. Sci. 111, E1327–E1333.
Guanter, L., Kaufmann, H., Segl, K., Foerster, S., Rogass, C., Chabrillat, S., Kuester, T., Hollstein, A., Rossner, G., Chlebek, C., 2015. The EnMAP spaceborne imaging spectroscopy mission for earth observation. Remote Sens. 7, 8830–8857.
Guo, J., Trotter, C.M., 2004. Estimating photosynthetic light-use efficiency using the photochemical reflectance index: variations among species. Funct. Plant Biol. 31, 255–265.
Hernández-Clemente, R., Navarro-Cerrillo, R.M., Suárez, L., Morales, F., Zarco-Tejada, P.J., 2011. Assessing structural effects on PRI for stress detection in conifer forests. Remote Sens. Environ. 115, 2360–2375.
Hernández-Clemente, R., Navarro-Cerrillo, R.M., Zarco-Tejada, P.J., 2012. Carotenoid content estimation in a heterogeneous conifer forest using narrow-band indices and PROSPECT+ DART simulations. Remote Sens. Environ. 127, 298–315.
Hernández-Clemente, R., Navarro-Cerrillo, R.M., Zarco-Tejada, P.J., 2014. Deriving predictive relationships of carotenoid content at the canopy level in a conifer forest using hyperspectral imagery and model simulation. IEEE Trans. Geosci. Remote Sens. 52, 5206–5217.
Hilker, T., Coops, N.C., Hall, F.G., Black, T.A., Chen, B., Krishnan, P., Wulder, M.A., Sellers, P.J., Middleton, E.M., Huemmrich, K.F., 2008. A modeling approach for upscaling gross ecosystem production to the landscape scale using remote sensing data. J. Geophys. Res. Biogeosci. 113.
Hill, J., Buddenbaum, H., Townsend, P.A., 2019. Imaging spectroscopy of Forest ecosystems: perspectives for the use of space-borne Hyperspectral earth observation systems. Surv. Geophys. 40, 553–588.
Holden, M., 1965. Chlorophylls. In: Goodwin, T.W. (Ed.), Chemistry and Biochemistry of Plant Pigments. Academic Press, London, pp. 641–688.
Horler, D.N.H., Dockray, M., Barber, J., Barringer, A.R., 1983. Red edge measurements for remotely sensing plant chlorophyll content. Adv. Space Res. 3, 273–277.
Houborg, R., Cescatti, A., Migliavacca, M., Kustas, W.P., 2013. Satellite retrievals of leaf chlorophyll and photosynthetic capacity for improved modeling of GPP. Agric. For. Meteorol. 177, 10–23.
Ingestad, T., 1971. A definition of optimum nutrient requirements in birch seedlings. II. Physiol. Plant. 24, 118–125.
Ingestad, T., 1979. Mineral nutrient requirements of *Pinus silvestris* and *Picea abies* seedlings. Physiol. Plant. 45, 373–380.
Ingestad, T., Lund, A., 1986. New concepts on soil fertility and plant nutrition as illustrated by research on forest trees and stands. Geoderma 40, 237–252.
Jacquemoud, S., Baret, F., 1990. PROSPECT: a model of leaf optical properties spectra. Remote Sens. Environ. 34, 75–91.
Jacquemoud, S., Verhoef, W., Baret, F., Bacour, C., Zarco-Tejada, P.J., Asner, G.P., François, C., Ustin, S.L., 2009. PROSPECT + SAIL models: a review of use for vegetation characterization. Remote Sens. Environ. 113, S56–S66.
Jay, S., Bendoula, R., Hadoux, X., Féret, J.-B., Gorretta, N., 2016. A physically-based model for retrieving foliar biochemistry and leaf orientation using close-range imaging spectroscopy. Remote Sens. Environ. 177, 220–236.
Kattenborn, T., Schiefer, F., Zarco-Tejada, P., Schmidtlein, S., 2019. Advantages of retrieving pigment content [µg/cm2] versus concentration [%] from canopy reflectance. Remote Sens. Environ. 230, 111195.
Kattge, J., Knorr, W., 2007. Temperature acclimation in a biochemical model of photosynthesis: a reanalysis of data from 36 species. Plant Cell Environ. 30, 1176–1190.
Knecht, M.F., Göransonn, A., 2004. Terrestrial plants require nutrients in similar proportions. Tree Physiol. 24, 447–460.
Le Maire, G., François, C., Soudani, K., Berveiller, D., Pontailler, J.-Y., Bréda, N., Genet, H., Davi, H., Dufrêne, E., 2008. Calibration and validation of hyperspectral indices for the estimation of broadleaved forest leaf chlorophyll content, leaf mass per area, leaf area index and leaf canopy biomass. Remote Sens. Environ. 112, 3846–3864.
Leuning, R., 1995. A critical appraisal of a combined stomatal-photosynthesis model for C3 plants. Plant Cell Environ. 18, 339–355.
Leuning, R., 1997. Scaling to a common temperature improves the correlation between the photosynthesis parameters J max and V cmax. J. Exp. Bot. 48, 345–347.
Long, S.P., Bernacchi, C.J., 2003. Gas exchange measurements, what can they tell us about the underlying limitations to photosynthesis? Procedures and sources of error. J. Exp. Bot. 54, 2393–2401.
Luther, J.E., Carroll, A.L., 1999. Development of an index of balsam fir vigor by foliar spectral reflectance. Remote Sens. Environ. 69, 241–252.
Malenovský, Z., Albrechtová, J., Lhotáková, Z., Zurita-Milla, R., Clevers, J., Schaepman, M.E., Cudlín, P., 2006. Applicability of the PROSPECT model for Norway spruce needles. Int. J. Remote Sens. 27, 5315–5340.
Marschner, H., 1995. Mineral Nutrition of Higher Plants, 2nd ed. Academic Press, London.
Masaitis, G., Mozgeris, G., Augustaitis, A., 2014. Estimating crown defoliation and the chemical constituents in needles of scots pine (Pinus sylvestris L.) trees by laboratory acquired hyperspectral data. Balt. For. 20, 314–325.
Mead, D.J., 2013. Sustainable Management of *Pinus radiata* Plantations. Food and agriculture organization of the United nations (FAO).
Medlyn, B.E., Dreyer, E., Ellsworth, D., Forstreuter, M., Harley, P.C., Kirschbaum, M.U.F., Le Roux, X., Montpied, P., Strassemeyer, J., Walcroft, A., 2002. Temperature response of parameters of a biochemically based model of photosynthesis. II. A review of experimental data. Plant Cell Environ. 25, 1167–1179.
Meroni, M., Rossini, M., Guanter, L., Alonso, L., Rascher, U., Colombo, R., Moreno, J., 2009. Remote sensing of solar-induced chlorophyll fluorescence: review of methods and applications. Remote Sens. Environ. 113, 2037–2051.
Middleton, E.M., Cheng, Y.-B., Hilker, T., Black, T.A., Krishnan, P., Coops, N.C., Huemmrich, K.F., 2009. Linking foliage spectral responses to canopy-level ecosystem photosynthetic light-use efficiency at a Douglas-fir forest in Canada. Can. J. Remote. Sens. 35, 166–188.
Mohammed, G.H., Colombo, R., Middleton, E.M., Rascher, U., van der Tol, C., Nedbal, L., Goulas, Y., Pérez-Priego, O., Damm, A., Meroni, M., 2019. Remote sensing of solar-induced chlorophyll fluorescence (SIF) in vegetation: 50 years of progress. Remote Sens. Environ. 231, 111177.
Mouazen, A.M., Kuang, B., De Baerdemaeker, J., Ramon, H., 2010. Comparison among principal component, partial least squares and back propagation neural network analyses for accuracy of measurement of selected soil properties with visible and near infrared spectroscopy. Geoderma 158, 23–31.
Nichol, C.J., Huemmrich, K.F., Black, T.A., Jarvis, P.G., Walthall, C.L., Grace, J., Hall, F.G., 2000. Remote sensing of photosynthetic-light-use efficiency of boreal forest. Agric. For. Meteorol. 101, 131–142.
Niinemets, Ü., Sack, L., 2006. Structural determinants of leaf light-harvesting capacity and photosynthetic potentials. Progr. Botany 385–419 (Springer).
Niinemets, Ü., Tenhunen, J.D., 1997. A model separating leaf structural and physiological effects on carbon gain along light gradients for the shade-tolerant species Acer saccharum. Plant Cell Environ. 20, 845–866.
North, P.R.J., 1996. Three-dimensional forest light interaction model using a Monte Carlo method. IEEE Trans. Geosci. Remote Sens. 34, 946–956.
NZFOA, 2018. 2018 Facts and Figures. New Zealand Plantation Forest Industry. New Zealand Forest Owners Association, Wellington, pp. 35.
Penuelas, J., Filella, I., Gamon, J.A., 1995. Assessment of photosynthetic radiation-use efficiency with spectral reflectance. New Phytol. 131, 291–296.
Peñuelas, J., Garbulsky, M.F., Filella, I., 2011. Photochemical reflectance index (PRI) and remote sensing of plant CO2 uptake. New Phytol. 191, 596–599.
Petisco, C., García-Criado, B., De Aldana, B.R.V., Zabalgogeazcoa, I., Mediavilla, S., 2005. Use of near-infrared reflectance spectroscopy in predicting nitrogen, phosphorus and calcium contents in heterogeneous woody plant species. Anal. Bioanal. Chem. 382, 458–465.
Porcar-Castell, A., Tyystjärvi, E., Atherton, J., Van der Tol, C., Flexas, J., Pfündel, E.E., Moreno, J., Frankenberg, C., Berry, J.A., 2014. Linking chlorophyll a fluorescence to photosynthesis for remote sensing applications: mechanisms and challenges. J. Exp. Bot. 65, 4065–4095.
Porder, S., Asner, G.P., Vitousek, P.M., 2005. Ground-based and remotely sensed nutrient availability across a tropical landscape. Proc. Natl. Acad. Sci. 102, 10909–10912.
Prikaziuk, E., van der Tol, C., 2019. Global sensitivity analysis of the SCOPE model in Sentinel-3 bands: thermal domain focus. Remote Sens. 11, 2424.
R Development Core Team, 2011. R: A Language and Environment for Statistical Computing. R Foundation for Statistical Computing, Vienna, Austria.
Raison, R.J., Myers, B.J., 1992. The biology of Forest growth experiment : linking water and nitrogen availability to the growth of *Pinus radiata*. For. Ecol. Manag. 52 (1–4), 279–308.
Rascher, U., Pieruschka, R., 2008. Spatio-temporal variations of photosynthesis: the potential of optical remote sensing to better understand and scale light use efficiency and stresses of plant ecosystems. Precis. Agric. 9, 355–366.

Rascher, U., Alonso, L., Burkart, A., Cilia, C., Cogliati, S., Colombo, R., Damm, A., Drusch, M., Guanter, L., Hanus, J., 2015. Sun-induced fluorescence–a new probe of photosynthesis: first maps from the imaging spectrometer HyPlant. Glob. Chang. Biol. 21, 4673–4684.
Reich, P.B., Schoettle, A.W., 1988. Role of phosphorus and nitrogen in photosynthetic and whole plant carbon gain and nutrient use efficiency in eastern white pine. Oecologia 77, 25–33.
Riaño, D., Vaughan, P., Chuvieco, E., Zarco-Tejada, P.J., Ustin, S.L., 2005. Estimation of fuel moisture content by inversion of radiative transfer models to simulate equivalent water thickness and dry matter content: analysis at leaf and canopy level. IEEE Trans. Geosci. Remote Sens. 43, 819–826.
Ripullone, F., Rivelli, A.R., Baraldi, R., Guarini, R., Guerrieri, R., Magnani, F., Peñuelas, J., Raddi, S., Borghetti, M., 2011. Effectiveness of the photochemical reflectance index to track photosynthetic activity over a range of forest tree species and plant water statuses. Funct. Plant Biol. 38, 177–186.
Rock, B.N., Hoshizaki, T., Miller, J.R., 1988. Comparison of in situ and airborne spectral measurements of the blue shift associated with forest decline. Remote Sens. Environ. 24, 109–127.
Schlerf, M., Atzberger, C., Hill, J., Buddenbaum, H., Werner, W., Schüler, G., 2010. Retrieval of chlorophyll and nitrogen in Norway spruce (Picea abies L. karst.) using imaging spectroscopy. Int. J. Appl. Earth Obs. Geoinf. 12, 17–26.
Scholten, R.C., Hill, J., Werner, W., Buddenbaum, H., Dash, J.P., Gallego, M.G., Rolando, C.A., Pearse, G.D., Hartley, R., Estarija, H.J., 2019. Hyperspectral VNIR-spectroscopy and imagery as a tool for monitoring herbicide damage in wilding conifers. Biol. Invasions 21, 3395–3413.
Sellers, P.J., Berry, J.A., Collatz, G.J., Field, C.B., Hall, F.G., 1992. Canopy reflectance, photosynthesis, and transpiration. III. A reanalysis using improved leaf models and a new canopy integration scheme. Remote Sens. Environ. 42, 187–216.
Serbin, S.P., Singh, A., McNeil, B.E., Kingdon, C.C., Townsend, P.A., 2014. Spectroscopic determination of leaf morphological and biochemical traits for northern temperate and boreal tree species. Ecol. Appl. 24, 1651–1669.
Sheriff, D.W., Nambiar, E.K.S., Fife, D.N., 1986. Relationships between nutrient status, carbon assimilation and water use efficiency in Pinus radiata (D. Don) needles. Tree Physiol. 2, 73–88.
Smith, W.K., Biederman, J.A., Scott, R.L., Moore, D.J.P., He, M., Kimball, J.S., Yan, D., Hudson, A., Barnes, M.L., MacBean, N., 2018. Chlorophyll fluorescence better captures seasonal and interannual gross primary productivity dynamics across dryland ecosystems of southwestern North America. Geophys. Res. Lett. 45, 748–757.
Stein, B.R., Thomas, V.A., Lorentz, L.J., Strahm, B.D., 2014. Predicting macronutrient concentrations from loblolly pine leaf reflectance across local and regional scales. GISci. Remote Sens. 51, 269–287.
Stylinski, C.D., Oechel, W.C., Gamon, J.A., Tissue, D.T., Miglietta, F., Raschi, A., 2000. Effects of lifelong [CO2] enrichment on carboxylation and light utilization of Quercus pubescens Willd. Examined with gas exchange, biochemistry and optical techniques. Plant Cell Environ. 23, 1353–1362.
Suárez, L., Zarco-Tejada, P.J., Sepulcre-Cantó, G., Pérez-Priego, O., Miller, J.R., Jiménez-Muñoz, J.C., Sobrino, J., 2008. Assessing canopy PRI for water stress detection with diurnal airborne imagery. Remote Sens. Environ. 112, 560–575.
Suárez, L., Zarco-Tejada, P.J., Berni, J.A.J., González-Dugo, V., Fereres, E., 2009. Modelling PRI for water stress detection using radiative transfer models. Remote Sens. Environ. 113, 730–744.
Taiz, L., Zeiger, E., Møller, I.M., Murphy, A., 2015. Plant Physiology and Development.
Tsay, M.-L., Gjerstad, D.H., Glover, G.R., 1982. Tree leaf reflectance: a promising technique to rapidly determine nitrogen and chlorophyll content. Can. J. For. Res. 12, 788–792.
Vasques, G.M., Grunwald, S., Sickman, J.O., 2008. Comparison of multivariate methods for inferential modeling of soil carbon using visible/near-infrared spectra. Geoderma 146, 14–25.
Verhoef, W., 1984. Light scattering by leaf layers with application to canopy reflectance modeling: the SAIL model. Remote Sens. Environ. 16, 125–141.
Verhoef, W., Jia, L., Xiao, Q., Su, Z., 2007. Unified optical-thermal four-stream radiative transfer theory for homogeneous vegetation canopies. IEEE Trans. Geosci. Remote Sens. 45, 1808–1822.
Verrelst, J., Rivera, J.P., van der Tol, C., Magnani, F., Mohammed, G., Moreno, J., 2015. Global sensitivity analysis of the SCOPE model: what drives simulated canopy-leaving sun-induced fluorescence? Remote Sens. Environ. 166, 8–21.
Vogelmann, T.C., 1993. Plant tissue optics. Annu. Rev. Plant Biol. 44, 231–251.
Walcroft, A.S., Whitehead, D., Silvester, W.B., Kelliher, F.M., 1997. The response of photosynthetic model parameters to temperature and nitrogen concentration in Pinus radiata D. Don. Plant Cell Environ. 20, 1338–1348.
Walker, A.P., Beckerman, A.P., Gu, L., Kattge, J., Cernusak, L.A., Domingues, T.F., Scales, J.C., Wohlfahrt, G., Wullschleger, S.D., Woodward, F.I., 2014. The relationship of leaf photosynthetic traits–Vcmax and Jmax–to leaf nitrogen, leaf phosphorus, and specific leaf area: a meta-analysis and modeling study. Ecol. Evol. 4, 3218–3235.
Wang, Z., Skidmore, A.K., Wang, T., Darvishzadeh, R., Hearne, J., 2015. Applicability of the PROSPECT model for estimating protein and cellulose+ lignin in fresh leaves. Remote Sens. Environ. 168, 205–218.
Wang, Z., Skidmore, A.K., Darvishzadeh, R., Wang, T., 2018. Mapping forest canopy nitrogen content by inversion of coupled leaf-canopy radiative transfer models from airborne hyperspectral imagery. Agric. For. Meteorol. 253, 247–260.
Watt, M.S., Coker, G., Clinton, P.W., Davis, M.R., Parfitt, R., Simcock, R., Garret, L., Payn, T.W., Richardson, B., Dunningham, A., 2005. Defining sustainability of plantation forests through identification of site quality indicators influencing productivity- a national view for New Zealand. For. Ecol. Manag. 216, 51–63.
Watt, M.S., Davis, M.R., Parfitt, R.L., 2009. Improved nutritional status of Cupressus lusitanica when grown adjacent to Pinus radiata. Can. J. For. Res. 39, 882–887.
Watt, M.S., Pearse, G.D., Dash, J.P., Melia, N., Leonardo, E.M.C., 2019. Application of remote sensing technologies to identify impacts of nutritional deficiencies on forests. ISPRS J. Photogramm. Remote Sens. 149, 226–241.
Weis, E., Berry, J.A., 1987. Quantum efficiency of photosystem II in relation to 'energy'-dependent quenching of chlorophyll fluorescence. Biochim. Biophys. Acta (BBA) Bioenergetics 894, 198–208.
Wong, C.Y.S., Gamon, J.A., 2015a. The photochemical reflectance index provides an optical indicator of spring photosynthetic activation in evergreen conifers. New Phytol. 206, 196–208.
Wong, C.Y.S., Gamon, J.A., 2015b. Three causes of variation in the photochemical reflectance index (PRI) in evergreen conifers. New Phytol. 206, 187–195.
Xu, L., Baldocchi, D.D., 2003. Seasonal trends in photosynthetic parameters and stomatal conductance of blue oak (Quercus douglasii) under prolonged summer drought and high temperature. Tree Physiol. 23, 865–877.
Yoder, B.J., Pettigrew-Crosby, R.E., 1995. Predicting nitrogen and chlorophyll content and concentrations from reflectance spectra (400–2500 nm) at leaf and canopy scales. Remote Sens. Environ. 53, 199–211.
Zarco-Tejada, P.J., Miller, J.R., Noland, T.L., Mohammed, G.H., Sampson, P.H., 2001. Scaling-up and model inversion methods with narrowband optical indices for chlorophyll content estimation in closed forest canopies with hyperspectral data. IEEE Trans. Geosci. Remote Sens. 39, 1491–1507.
Zarco-Tejada, P.J., Miller, J.R., Harron, J., Hu, B., Noland, T.L., Goel, N., Mohammed, G.H., Sampson, P., 2004a. Needle chlorophyll content estimation through model inversion using hyperspectral data from boreal conifer forest canopies. Remote Sens. Environ. 89, 189–199.
Zarco-Tejada, P.J., Miller, J.R., Morales, A., Berjón, A., Agüera, J., 2004b. Hyperspectral indices and model simulation for chlorophyll estimation in open-canopy tree crops. Remote Sens. Environ. 90, 463–476.
Zarco-Tejada, P.J., Catalina, A., González, M.R., Martín, P., 2013a. Relationships between net photosynthesis and steady-state chlorophyll fluorescence retrieved from airborne hyperspectral imagery. Remote Sens. Environ. 136, 247–258.
Zarco-Tejada, P.J., González-Dugo, V., Williams, L.E., Suárez, L., Berni, J.A.J., Goldhamer, D., Fereres, E., 2013b. A PRI-based water stress index combining structural and chlorophyll effects: assessment using diurnal narrow-band airborne imagery and the CWSI thermal index. Remote Sens. Environ. 138, 38–50.
Zarco-Tejada, P.J., González-Dugo, M.V., Fereres, E., 2016. Seasonal stability of chlorophyll fluorescence quantified from airborne hyperspectral imagery as an indicator of net photosynthesis in the context of precision agriculture. Remote Sens. Environ. 179, 89–103.
Zarco-Tejada, P.J., Camino, C., Beck, P.S.A., Calderon, R., Hornero, A., Hernández-Clemente, R., Kattenborn, T., Montes-Borrego, M., Susca, L., Morelli, M., 2018. Previsual symptoms of Xylella fastidiosa infection revealed in spectral plant-trait alterations. Nat. Plants 4, 432–439.
Zarco-Tejada, P.J., Hornero, A., Beck, P.S.A., Kattenborn, T., Kempeneers, P., Hernández-Clemente, R., 2019. Chlorophyll content estimation in an open-canopy conifer forest with sentinel-2A and hyperspectral imagery in the context of forest decline. Remote Sens. Environ. 223, 320–335.
Zhang, Q., Xiao, X., Braswell, B., Linder, E., Baret, F., Moore Iii, B., 2005. Estimating light absorption by chlorophyll, leaf and canopy in a deciduous broadleaf forest using MODIS data and a radiative transfer model. Remote Sens. Environ. 99, 357–371.